UNIVERSIDAD DE CHILE
FACULTAD DE CIENCIAS FÍSICAS Y MATEMÁTICAS
DEPARTAMENTO DE INGENIERÍA CIVIL

ESTIMACIÓN MULTIDECADAL DEL APORTE HIDROLÓGICO Y BALANCE DE MASA GLACIAR EN LOS ANDES SEMIÁRIDOS A PARTIR DE MODELAMIENTO DE BASE FÍSICA Y BALANCES DE MASA GEODÉSICOS

TESIS PARA OPTAR AL GRADO DE MAGÍSTER EN CIENCIAS DE LA INGENIERÍA, MENCIÓN RECURSOS Y MEDIO AMBIENTE HÍDRICO

ALONSO MEJÍAS ACUÑA

PROFESOR GUÍA:

JAMES MCPHEE TORRES

MIEMBROS DE LA COMISIÓN:

ALFONSO FERNANDEZ RIVERA

DAVID FARÍAS BARAHONA

SANTIAGO MONTSERRAT MICHELINI

SANTIAGO DE CHILE

Esta tesis fue parcialmente financiada por ANID a través del proyecto FONDECYT 1201429 y la beca ANID-MAGISTER NACIONAL 2021 folio 22211060.

2023

RESUMEN DE LA TESIS PARA OPTAR AL GRADO DE: Magíster en Ciencias de la Ingeniería, mención Recursos y Medio Ambiente Hídrico
POR: Alonso Mejías Acuña
FECHA: 2023
PROFESOR GUIA: James McPhee Torres

ESTIMACIÓN MULTIDECADAL DEL APORTE HIDROLÓGICO Y BALANCE DE MASA GLACIAR EN LOS ANDES SEMIÁRIDOS A PARTIR DE MODELAMIENTO DE BASE FÍSICA Y BALANCES DE MASA GEODÉSICOS

Los glaciares son de suma importancia en diversos entornos, y debido al acelerado retroceso experimentado en las últimas décadas, se han intensificado los esfuerzos por lograr una comprensión integral de sus variables clave como el balance de masa y el derretimiento glaciar. Sin embargo, la escasez de datos en regiones de difícil acceso, como los Andes, dificultan los estudios que quieran abarcar un largo periodo histórico. Esta investigación examina el balance de masa y el deshielo del Glaciar Universidad desde 1955 hasta 2020, al mismo tiempo que evalúa la influencia en las magnitudes y tendencias encontradas al incorporar balances de masa geodésicos. Utilizando el Modelo CRHM, desarrollamos un modelo hidro-glaciológico físicamente basado del Glaciar Universidad, el más grande de los Andes Semiaridos. La calibración del modelo se realizó con balances de masa geodésicos disponibles entre 1955 hasta 2020, mientras que la validación se llevó a cabo a través de observaciones en terreno entre los años 2012 y 2014.

A través de un análisis de puntos de cambio se encontraron tres períodos distintos en la evolución del balance de masa: uno de perdida significativa en los 1955-1971 y 2006-2020, y un periodo cercano al equilibrio entre 1971-2006. Estos períodos concuerdan con las fases observadas de la Oscilación Decadal del Pacífico y los eventos de El NIÑO. Al analizar la escorrentía proveniente de la fusión del hielo y neviza, encontramos una tendencia positiva del 8% por década en la contribución del Glaciar Universidad desde 1971. Al comparar versiones sin calibrar y calibradas del modelo desarrollado, se encontraron los mismos patrones de variabilidad temporal. Sin embargo, los balances de masa acumulados calculados mostraron las mayores diferencias: el modelo calibrado entre 2000 al 2020 sobrestimó la pérdida de masa en un 34%, mientras que el modelo no calibrado sobrestimó en un 58%. En contraste, el modelo calibrado entre 1955 hasta 2020 mostró una sobreestimación mínima del 0.1% en la pérdida de masa. Además, este modelo demostró una representación ligeramente mejorada del albedo anual.

TABLA DE CONTENIDO

I. INTRODUCCIÓN

A lo largo del último siglo, los glaciares en todo el mundo han experimentado un retroceso generalizado. Sin embargo, en las últimas décadas, esta pérdida de masa se ha acelerado significativamente (Zemp et al., 2015; 2019). La disminución del volumen de los glaciares ha resultado en varios impactos, incluida una reducción del caudal en regiones montañosas, lo que conlleva una menor capacidad para mitigar las sequías (Utlee et al., 2022). Además, la reducción de los glaciares contribuye al aumento del nivel del mar (Zemp et al., 2019) e intensifica los riesgos naturales como las inundaciones por desbordamiento de lagos glaciares (Ahmed et al., 2021). Estas consecuencias ya se están observando y se proyecta que sus efectos aumentarán en el futuro (IPCC, 2022).

En la región de los Andes Centrales de Chile, los glaciares desempeñan un papel crucial en garantizar la disponibilidad de suministro de agua para áreas densamente pobladas, regiones agrícolas productivas y zonas montañosas involucradas en la minería y la producción de energía hidroeléctrica. Si bien el deshielo de nieve sirve como fuente principal de agua dulce, el deshielo glaciar contribuye de manera significativa, especialmente durante el final del verano y en años de sequía (Ayala et al., 2020). Un ejemplo es la contribución de la escorrentía glaciar al total del caudal del Río Maipo, la principal fuente de agua dulce para Santiago, la capital y ciudad más poblada de Chile. Durante los primeros años de la megasequía (Boisier et al., 2016) entre el 2010 y el 2015, el deshielo glaciar llegó a representar un 17% del caudal anual del Río Maipo y un 55% de la escorrentía de verano (Ayala et al., 2020).

En las últimas décadas, ha habido un aumento significativo en el número de estudios y conocimiento sobre la criósfera andina, incluyendo los glaciares ubicados en la Región de los Andes Centrales de Chile y Argentina (Masiokas et al., 2020). Estudios utilizando técnicas de teledetección han registrado consistentemente el retroceso de los glaciares en los Andes chilenos. Por ejemplo, Barcaza et al, (2018) encontraron una reducción de 92.3 km^2 en el área de glaciares blancos entre 2000 y 2015, mientras que el área de glaciares cubiertos y rocosos se mantuvo aparentemente sin cambios. Otros estudios han desarrollado balances de masa geodésicos por medio de imágenes ópticas (Dussaillant et al., 2019) o imágenes de radar (Braun et al., 2019) para cuantificar el balance de masa a escala regional. Braun et al, (2019) y Dussaillant et al, (2019) determinaron que los glaciares andinos aportaron aproximadamente el 10% del total de la contribución glaciar (excluyendo a la Antártida y Groenlandia) al aumento del nivel del mar entre 2002 y 2016, mientras que Hugonnet et al. (2021) estimo la contribución de los Andes Sur en un 8% del total global entre los años 2000-2019. Además, Dussaillant et al, (2019) encontró que los Andes áridos experimentaron un balance de masa cercano al equilibrio entre 2000 y 2009, pero pérdidas significativas de masa entre 2009 y 2018. También se han realizado estudios de modelamiento para cuantificar el derretimiento glaciar y su aporte hídrico a nivel de cuenca (Peña & Nazara, 1987; Burger et al., 2018; Ayala et al., 2020) o para proyectar escenarios futuros bajo el cambio climático, centrándose en escalas locales (Ragettli et al., 2016; Escanilla-Minchel et al., 2020) o abarcando los Andes Centrales en estudios globales (Huss & Hock, 2018). Estas

proyecciones indican consistentemente una pérdida significativa de masa glaciar en el futuro, lo que conduce a una disminución en el total del deshielo de las cuencas de los Andes semiáridos y un máximo anticipado en la escorrentía anual (Ragettli et al., 2016; Huss & Hock, 2018).

Existen distintos enfoques para modelar el derretimiento de la nieve y glaciares que son empleados por las diferentes plataformas de modelamiento glaciar. El índice grado-día consiste en establecer una relación empírica de carácter lineal entre la temperatura del aire y el derretimiento, por lo que solo requiere como entrada meteorológica la temperatura y precipitación. Los bajos requerimientos en términos computacionales y meteorológicos de este tipo de modelo han resultado útiles para modelos glaciares a escala regional o global como GloGEM (Huss & Hock, 2015) u Open Global Glacier Model (Maussion et al., 2019). Algunos modelos modifican el índice grado-día considerando otras variables, por ejemplo, el índice grado-día mejorado (Pellicciotti et al., 2005) que también considera la radiación de onda corta y el albedo de la nieve. Este enfoque ha sido empleado por el modelo TOPKAPI-ETH (Fatichi et al., 2014; Ragettli et al., 2016), permitiendo mejorar el desempeño de un modelo grado-día, agregando solamente una entrada meteorológica (Pellicciotti et al., 2005). Por otro lado, el balance de energía resulta ser el de mayor complejidad, ya que resuelve de manera explícita las ecuaciones de balance energético y másico, calculando las tasas de derretimiento a partir de la energía disponible para este proceso. Este enfoque requiere una mayor cantidad de datos meteorológicos, incluyendo la temperatura del aire, precipitación, radiación neta de onda corta y larga. Los modelos de balance de energía usualmente son utilizados para desarrollar modelos enfocados a escala de cuenca, glaciar o puntual. Ejemplos de plataformas de modelación que utilicen este enfoque son los modelos DHSVM-GDN (Naz et al., 2014), CRHM (Pomeroy et al., 2007), y COSIPY v1.3 (S

En el presente estudio, se emplea la plataforma de modelación Cold Region Hydrological Model (CRHM) debido a que la representación físicamente basada de los distintos procesos hidrológicos permite suponer que los parámetros permanecerán estables en el tiempo. Esto lo convierte en una opción adecuada para estudios que abarcan largos periodos de modelación, donde se evidencian distintos periodos hidroclimáticos. A diferencia de lo que podría ocurrir con modelos que dependen en mayor grado de la calibración de parámetros, como por ejemplo los modelos grado-día (Huss et al., 2009). Además, la discretización a escala de Unidades de Respuesta Hidrológica (URH) de CRHM, enfocada principalmente en el desarrollo de modelos a escala de cuenca, lo hacen adecuado para los modelos a escala glaciar y sus laderas tributarias. Esto permite reducir el costo computacional que conllevaría un modelo distribuido, manteniendo la representatividad de los procesos a escala de URH.

Es relevante mencionar que el modelo CRHM ha sido usado exitosamente en diferentes regiones glaciarizadas (Pomeroy et al., 2022). Por ejemplo, Krogh et al., (2015) estudio la cuenta altamente glaciarizada (17.5% de área glaciar) del río Baker en la Patagonia Chilena. Su estudio se enfoco en identificar los procesos hidrológicos predominantes in la región, revelando que el flujo subsuperficial constituye uno de los flujos principales para el Río Baker, representando el 68.5% de la escorrentía. Krogh et al., (2015) también encontró que la lluvia es la principal fuete de escorrentía, siendo aproximadamente tres veces la

contribución proveniente del derretimiento de la nieve y hielo. En otro estudio, Fang & Pomeroy (2023) investigaron las consecuencias de los cambios en el área glaciar in las cabeceras del río Bow en las Montañas Rocosas de Canadá. Sus descubrimientos indican que, bajo un clima más cálido, habrá una reducción de la escorrentía glaciar debido a la menor área glaciarizada. A pesar del decrecimiento a la escorrentía glaciar, la cuenca experimentara un aumento en su caudal debido a un incremento en las lluvias de invierno, adelantando el máximo anual.

Debido a la falta de datos meteorológicos y observaciones que permitan la calibración y validación de resultados, existen relativamente pocos estudios de modelación hidro-glaciológica, en relación con los estudios de carácter observacional (Pellicciotti et al., 2014). Especialmente, se han realizado pocos estudios que abarquen periodos de varias décadas. Esta limitación resulta clave para poder comprender cómo han ido cambiando los balances de masa o la escorrentía glaciar a lo largo del tiempo y cómo podrían alterarse en distintos escenarios de cambio climático.

En los Andes semiáridos (32-34ºS), el concepto de "peak water" ha sido poco estudiado. Este término que hace referencia al período a largo plazo en el que el glaciar entrega el máximo volumen de deshielo debido a un fuerte estado de desequilibrio. Aunque existe una percepción de que la máxima contribución de escorrentía glaciar ya se ha alcanzado o se alcanzará en las próximas décadas a escala regional (Huss & Hock, 2018), no hay claridad sobre este comportamiento a nivel de cuenca. La información sobre este fenómeno es crucial para tomar decisiones informadas en términos de mitigación y adaptación en el contexto del cambio climático (Ayala et al., 2020).

En los Andes semiáridos, los estudios glaciológicos que han examinado la evolución glaciar durante períodos de al menos varías décadas se han centrado principalmente en la cuenca del Maipo (Masiokas et al., 2016; Farías-Barahona et al., 2019; Ayala et al., 2020). Por ejemplo, Masiokas et al. (2016) desarrollaron un modelo de balance de masa superficial del glaciar Echaurren norte. El glaciar Echaurren Norte, ubicado en la cuenca del Río Maipo, es el glaciar con el registro de balance de masa más extenso del hemisferio sur, efectuado desde 1975 hasta la actualidad (Escobar, 1995). Utilizando datos de estaciones meteorológicas, fluviométricas y mediciones de SWE, Masiokas et al. (2016) reconstruyeron el balance de masa glaciar desde 1909. El estudio reveló una tendencia negativa en el balance de masa, interrumpido por tres períodos positivos en las décadas de 1920, 1980 y a principios de la década del 2000. Por otro lado, Farías-Barahona et al. (2019) utilizaron una combinación de mapas topográficos, modelos de elevación obtenidos desde la misión topográfica Shuttle Radar y productos LiDAR para estimar el balance de masa geodésico del glaciar Echaurren Norte entre 1955 y el 2020. Sus hallazgos son generalmente consistentes con los resultados obtenidos por Masiokas et al. (2016) y los balances de masa glaciológicos registrados. Además, Farías-Barahona et al. (2019) investigaron la relación entre el balance de masa y el fenómeno El NIÑO-Oscilación del Sur (ENSO), revelando una correlación entre las fases positivas (negativas) de ENSO y los años caracterizados por balances de masa positivos (negativos). El trabajo de Ayala et al. (2020) es el estudio más extenso realizado en los Andes semiáridos para estimar la escorrentía glaciar y cuantificando su contribución en la cuenca

del Río Maipo, abarcando desde 1955 al 2015. Ayala et al. (2020) calibraron los parámetros relacionados con la nieve utilizando imágenes MODIS y reconstrucciones de equivalente de aguanieve, mientras que para los parámetros relacionados a la fusión de hielo glaciar se utilizaron balances de masa geodésicos (BMG) entre los periodos 1955-2000 y 2000-2013. Ayala et al. (2020) identificaron una tendencia negativa en el balance de masa, con períodos ocasionales cercanos al equilibrio o ligeramente positivos, especialmente a inicios de la década del 2000. Además, respecto a la escorrentía glaciar encontraron una disminución en los máximos de la contribución glaciar al caudal total de la cuenca desde el año 1968/1969 donde se registró la mayor contribución.

En los últimos años, el uso de balances de masa geodésicos obtenidos a partir de sensores satelitales o fotogrametría ha permitido calcular los cambios en el volumen de los glaciares y estimar los balances de masa a través de distintos supuestos sobre la densidad del hielo. Esta metodología ha ampliado significativamente la cobertura temporal y espacial de los estudios de balance de masa glaciar (Braithwaite & Hughes, 2020), pasando de tener disponibles solo algunos glaciares con balances geodésicos o mediciones glaciológicas a una cobertura casi global (Berthier et al., 2023). Por ejemplo, los estimados de diferencia de elevación del hielo generadas por Hugonnet et al. (2021) y Dusaillant et al. (2020) utilizando imágenes ASTER han permitido a distintos investigadores desarrollar sus trabajos según sus necesidades específicas (Barandun et al., 2022; Compagno et al., 2022; McCarthy et al., 2023; Li et al., 2023; Rounce et al., 2023). Sin embargo, es importante mencionar que existen diferencias entre los estimados regionales de los distintos grupos de investigación y métodos disponibles (Hugonnet et al., 2021; Berthier et al., 2023). Las causas y consecuencias de las discrepancias encontradas aún no se encuentran claras, aunque ya existen iniciativas enfocadas en resolverlas, como por ejemplo el proyecto GlaMBIE (Berthier and others, 2023).

La mayoría de las técnicas para obtener balances de masa geodésicos, debido a las fechas de despliegue de los sensores utilizados, la mayoría de las estimaciones de B.M.G están disponibles con posterioridad al año 2000 (Berthier et al., 2023, tabla 3). Sin embargo, los balances de masa geodésicos obtenidos a partir de diferencias de modelos de elevación digital generados a través de imágenes estereoscópicas ópticas presentan la posibilidad de generar estudios de balances de masa que abarquen largos periodos de tiempo, incluso desde la década de los 60. No obstante, está técnica aún posee distintos desafíos como las limitaciones correspondientes a su cobertura espacial está sujeta a estudios locales y problemas potenciales debido a la cobertura de nubes, falta de contraste especialmente en el área de acumulación, dificultad para encontrar terrenos estables que actúen cómo punto de control, y la alta posibilidad de que las imágenes no hayan sido adquiridas al final del año hidrológico (Berthier et al., 2023).

En los Andes semiáridos los balances de masa geodésicos cobran una especial relevancia, considerando que los balances de masa a través del método glaciológico son limitados debido a las complicaciones logísticas y los costos asociados (Farías-Barahona et al., 2020). A pesar de la gran oportunidad que representan, aún existe un limitado número de estudios que los utilicen. Por ejemplo, Barandun et al. (2022) utilizaron los cambios de elevación de Hugonnet

et al. (2021) para calibrar la temperatura umbral de un modelo mejorado de grado-día. De manera similar, Ayala et al. (2020) utilizaron balances de masa geodésicos generados por Braun et al. (2019) y extendidos por Farias-Barahona et al. (2019) para calibrar la fusión del hielo en el modelo TOPKAPI-ETH.

El Glaciar Universidad (34°40'S, 70°20'W), ubicado en los Andes semiáridos, en la cabecera del Río Tinguiririca, es el glaciar más grande al norte de la Patagonia, con un área de 26.3 km^2 y una elevación media de 3683 m.s.n.m según la Dirección General de Aguas (DGA, 2022). Debido a su tamaño relativamente grande en comparación con otros glaciares de la región, el Glaciar Universidad juega un papel importante como recurso hídrico a nivel de cuenca, por ejemplo, durante el verano de 2010/2011 solo el glaciar Universidad contribuyó con un 10~13% del caudal total de la cuenca del Río Tinguiririca en Bajo los Briones (Bravo et al., 2017). A punto de comparación, todos los glaciares de la Cuenca del Río Maipo aportaron un 55% de la escorrentía de verano del Río Maipo entre los años 2010-2015 (Ayala et al., 2020). La contribución hídrica del glaciar Universidad y los demás glaciares de Chile Central (30-38ºS) se vuelve especialmente relevante en el contexto de la megasequía. Desde el año 2010 en Chile central se han experimentado años consecutivos con déficit de precipitaciones entre el 20 y 40%, produciendo un decrecimiento del manto de nieve y escorrentía.

El Glaciar Universidad ha sufrido una serie de avances y retrocesos desde el primer registro efectuado por Lliboutry (1958), quien reportó un avance súbito alrededor de 1943, seguido de una fuerte recesión cercana a un kilómetro en la parte baja entre los años 1946 y 1950. La Dirección General de Aguas (DGA), a través de un análisis de imágenes satelitales y fotografías áreas para distintos glaciares en todo Chile, encontró que el glaciar Universidad ha experimentado una reducción de un 6% de su área entre 1945 y 2011 (DGA, 2011). Esta reducción es comparativamente menor que la observada en otros glaciares de tamaño similar en los Andes semiáridos. Por ejemplo, el glaciar Juncal Sur, Olivares Alfa, Olivares Beta y Olivares Gamma han perdido un 34%, 32%, 37% y un 20% respectivamente. Wilson et al. (2016) investigó las fluctuaciones de la velocidad superficial del hielo entre 1967 y 2015, observando un aumento significativo entre 1967 y 1987, seguido por una fuerte desaceleración entre entre 1987 y 2015. Dos periodos relativamente cortos de aceleración fueron identificados entre 1993 a 1997 y entre 2002 a 2008. Con base en sus resultados, sugieren que el glaciar puede haber experimentado periodos de balance de masa negativos desde 1987, con periodos levemente positivos entre 1993-1997 y 2002-2008. Es importante señalar que la hipótesis no resulta concluyente, ya que los cambios en la velocidad superficial del hielo también pueden ser atribuidos a diferentes etapas de un ciclo de surgencia (Wilson et al., 2016). Durante los años 2012 al 2014, Kinnard et al. (2018) realizó una extensa campaña de monitoreo sobre el glaciar Universidad, encontrando que, del balance de masa del glaciar, aproximadamente de un 3% a 6% corresponden a sublimación, un resultado en coherencia a lo indicado por Bravo et al. (2017).

Respecto a la contribución hidrológica del Glaciar Universidad, Bravo et al. (2017) utilizó un modelo grado-hora previamente calibrado y un modelo de balance de energía para calcular el aporte de la escorrentía del Glaciar Universidad a la cuenca Tinguiririca en Bajo los Briones. Sus resultados indicaron que para el año 2010, el derretimiento glaciar aportó entre un 10% a 13% en la temporada de ablación (diciembre a marzo). Por otro lado, Escanilla-

Minchel et al. (2020) empleó un modelo grado-día para proyectar la escorrentía y volumen glaciar para el periodo 2008-2100 bajo dos escenarios de cambio climático, RCP 4.5 y RCP 8.5. Sus hallazgos indican un decrecimiento significativo en la escorrentía glaciar, con disminuciones estimadas entre un 25 y 68% bajo el escenario RCP 4.5, y entre un 51-84% bajo el escenario RCP 8.5. Además, Escanilla-Minchel et al. (2020) proyecta la ocurrencia del "peak water" alrededor del año 2040.

Nuestro trabajo permite entender de mejor manera la evolución del glaciar Universidad, abarcando un periodo histórico poco estudiado desde el modelamiento debido a la escasez de los datos necesarios.

El presente estudio a través del modelamiento hidro-glaciológico tiene como objetivo estimar el balance de masa y la escorrentía del Glaciar Universidad en el periodo 1955-2020. Permitiendo encontrar los distintos puntos de cambio, tendencias y relaciones con fenómenos climáticos de estas variables. Por otro lado, se estudian los beneficios de incorporar en el proceso de calibración balances de masa geodésicos en la simulación de largo plazo de la evolución glaciar, especialmente en el balance de masa acumulado

Por lo tanto, este trabajo de tesis considera las siguientes preguntas de investigación:

1. ¿Cómo ha evolucionado el balance de masa glaciar y la escorrentía del glaciar Universidad durante los últimos 60 años?
2. ¿Cuáles son los beneficios e implicancias de utilizar balances de masa geodésicos de larga data al calibrar un modelo hidro-glaciológico?

Con el fin de responder dichas preguntas, se desarrolló un modelo hidro-glaciológico de base física del glaciar Universidad a través de la plataforma Cold Regions Hydrological Model (CRHM). Se compararon los resultados de tres casos: un modelo sin calibrar, otro calibrado con balances de masa geodésicos obtenidos entre 2000 y 2020, y un tercer caso calibrado con balances de masa geodésicos entre 1955-2020. El análisis histórico de las variables glaciares analizadas: balances de masa, escorrentía, albedo y línea de equilibrio altitudinal, se realizó buscando tendencias estadísticamente significativas y puntos de cambio.

1.1. Objetivos

El objetivo general del presente estudio es el siguiente:

1.1.1. Objetivos Generales

Caracterizar y comprender los procesos que determinan la evolución glaciológica del glaciar universidad en el periodo 1955-2020.

1.1.2. Objetivos Específicos

- Analizar la evolución del balance de masa, escorrentía, línea de equilibrio altitudinal y albedo del glaciar Universidad durante el periodo de estudio (1955 al 2020).

- Cuantificar las diferencias en las series históricas y en el desempeño de los distintos casos generados al utilizar balances de masa geodésicos en la calibración del modelo CRHM.
- Analizar los beneficios de incorporar balances de masa geodésicos en la calibración de un modelo hidro-glaciológico en simulaciones de largo plazo.

1.2. Datos y Metodología

Para el proceso de calibración del modelo hidro-glaciológico CRHM se utilizaron balances de masa geodésicos generados a partir de procedimientos fotogramétricos generados por Mahmoud et al. (2022) y los cambios de elevación en la superficie del hielo de Hugonett et al. (2021).

Se emplearon para la generación de las forzantes el producto grillado CR2met (Boisier et al., 2016), el reanálisis ERA5 Land (Hersbach et al., 2020) y las mediciones de la estación meteorológica automática de la campaña de monitoreo de Kinnard et al (2018).

Para modelar la evolución de las distintas variables glaciares de interés se generó un modelo hidro-glaciológico del glaciar Universidad y sus laderas tributarias en la plataforma de modelación CRHM (Pomeroy 2007, Pradhananga and Pomeroy 2022).

Se generaron tres casos de estudio a partir del modelo generado: un caso sin calibrar, un modelo calibrado solo con BMG entre 2000 y 2020, y un modelo calibrado con BMG entre 1955 y 2020.

II. ARTÍCULO PARA PUBLICACIÓN

A continuación, se presenta el artículo titulado "*Multidecadal estimation of hydrological contribution and glacier mass balance in the semi-arid Andes based on physically-based modeling and geodetic mass balances*":

Multidecadal estimation of hydrological contribution and glacier mass balance in the semi-arid Andes based on physically-based modeling and geodetic mass balances

Alonso Mejías[1,2], James McPhee[1,2], Alfonso Fernandez[3], Hazem Mahmoud[4] and David Farías-Barahona[3]
[1]Department of Civil Engineering, Universidad de Chile, Santiago, Chile.
[2]Advanced Mining Technology Center (AMTC), Universidad de Chile, Santiago, Chile.
[3]Department of Geography, Universidad de Concepción, Concepción, Chile.
[4]Department of Environmental and Civil Engineering, University of Texas, San Antonio, USA.

Abstract

Glaciers are of paramount importance in diverse environments, and due to the accelerated retreat experienced in recent decades, efforts have intensified to achieve a comprehensive understanding of key variables such as mass balance and glacial melting. However, the scarcity of data in regions that are difficult to access, such as the Andes, makes it difficult for studies to cover a long historical period. This research examines the mass balance and melting of the University Glacier from 1955 to 2020, while assessing the influence on the magnitudes and trends found by incorporating geodetic mass balances. Using the CRHM Model, we developed a physically based hydro-glaciological model of the Universidad Glacier, the largest in the Semiarid Andes. Model calibration was performed with geodetic mass balances available between 1955 to 2020, while validation through on-site observations between the years 2012 and 2014.

Change point analysis revealed three periods: significant loss from 1955-1971 and 2006-2020, and near equilibrium from 1971-2006. These periods align with the Pacific Decadal Oscillation and El Niño events. The runoff from ice melt showed a positive trend of 8% per decade since 1971. Comparing models, both calibrated and uncalibrated showed the same periods and trends. However, cumulative mass balances differed significantly: the model calibrated from 2000 to 2020 overestimated mass loss by 34%, while the uncalibrated model overestimated by 58%. The model calibrated from 1955 to 2020 had a minimal overestimation of 0.1% in mass loss and slightly improved representation of annual albedo.

1. Introduction

In the Central Andes region of Chile, glaciers play a crucial role in ensuring the availability of water supply for densely populated areas, productive agricultural regions, and mountainous areas involved in mining and hydroelectric power production. While snowmelt serves as the main source of freshwater, glacier melt contributes significantly, especially during late summer and in drought years (Ayala and others, 2020). An example is the contribution of glacier runoff to the total flow of the Maipo River, the main source of freshwater for Santiago, the capital, and the most populous city of Chile. During the early years of the megadrought (Boisier and others, 2016) between 2010 and 2015, glacier melt accounted for 55% of the summer flow of the Maipo River (Ayala and others, 2020).

In recent decades, there has been a significant increase in the number of studies and knowledge about the Andean cryosphere, including glaciers located in the Central Andes region (Masiokas and others, 2020). Studies using remote sensing techniques have consistently recorded the retreat of glaciers in the Chilean Andes. For example, Barcaza and others (2018) found a reduction of 92.3 km2 in the area of white glaciers between 2000 and 2015, while the area of debris-covered and rock glaciers remained seemingly unchanged. Other studies have developed geodetic mass balances using optical imagery (Dussaillant and others, 2019) or radar images (Braun and others, 2019) to quantify the regional-scale mass balance. Braun and others (2019) and Dussaillant and others (2019) determined that Andean glaciers contributed approximately 10% of the total glacier contribution, excluding Antarctica and Greenland, to the global sea-level rise between 2002 and 2016. Furthermore, Dussaillant and others (2019) found that the arid Andes experienced a near-balanced mass balance between 2000 and 2009 but significant mass losses between 2009 and 2018. Modeling studies have also been conducted to quantify glacier melting and its hydrological contribution at the watershed level (Peña and Nazara, 1987; Burger and others, 2018; Ayala and others, 2020) or to project future scenarios under climate change, focusing on local scales (Ragettli and others, 2016; Escanilla-Minchel and others, 2020) or encompassing the Central Andes in global studies (Huss and Hock, 2018). These projections consistently indicate a significant loss of glacier mass in the future, leading to a decrease in total meltwater from the semi-arid Andean basins and an anticipation of a few months in the annual maximum value of annual runoff (Ragettli and others, 2016; Huss and Hock, 2018).

There are different approaches to model snow and glacier melting used by various glacier modeling platforms. The degree-day index method consists of establishing an empirical linear relationship between air temperature and melting, thus requiring only temperature and precipitation as meteorological inputs. Its low computational and meteorological requirements have proven useful for regional or global-scale glacier models like GloGEM (Huss & Hock, 2015) and Open Global Glacier Model (Maussion and others, 2019). Some models modify the degree-day index by considering other variables, for example, the enhanced degree-day index (Pellicciotti and others, 2005), which also takes shortwave radiation and snow albedo into account. This approach has been employed by the TOPKAPI-ETH model (Fatichi and others, 2014; Ragettli and others, 2016), allowing for improved

performance of a degree-day model by adding only one meteorological input (Pellicciotti and others, 2005). On the other hand, the energy balance approach is the most complex, explicitly solving the energy and mass balance equations to calculate melting rates based on the available energy for this process. This approach requires a larger amount of meteorological data, including air temperature, precipitation, net shortwave, and longwave radiation. Energy balance models are usually used to develop models focused on the watershed, glacier, or point scale. Examples of modeling platforms that use this approach are DHSVM-GDN (Naz and others, 2014), CRHM (Pomeroy and others, 2007), and COSIPY v1.3 (Sauter, 2020).

In the present study, the Cold Region Hydrological Model (CRHM) is employed because its physically based representation of different hydrological processes allows us to assume that the parameters will remain stable over time. This makes it a suitable option for studies covering long modeling periods, where different hydroclimatic periods are evident. Unlike models that rely more heavily on parameter calibration, such as degree-day models (Huss and others, 2009), CRHM's discretization at the scale of Hydrological Response Units (HRUs) is primarily focused on developing watershed-scale models, making it suitable for glacier and its tributary slopes modeling. This allows for a reduction in computational cost that would be associated with a distributed model while maintaining the representativeness of processes at the HRU scale.

It is relevant to mention that the CRHM model has already been successfully used in different glacierized regions (Pomeroy and others, 2022). For example, Krogh and others (2015) studied the highly glacierized basins (17.5% glacier area) of the Baker River in Chilean Patagonia. Their study focused on identifying the dominant hydrological processes in the region, revealing that sub-surface flow constitutes the primary driver of runoff in the Baker River, accounting for 68.5%. Also, they found that rainfall serves as the main source of runoff, being nearly three times greater than the contribution of ice and snowmelt. In another study, Fang & Pomeroy (2023) explored the consequences of changes in glacier area in the headwater basin of the Bow River in the Rocky Mountains of Canada. Their findings indicate that, under a warmer climate scenario, there will be a reduction in glacier melt due to diminished glacier coverage. However, owing to increased rainfall during winter months, the basin is projected to experience a rise in annual runoff and an earlier peak in the season.

Due to the lack of meteorological data and observations that allow for calibration and validation of results, there are relatively few hydro-glaciological modeling studies compared to observational studies (Pellicciotti and others, 2014). Particularly, there have been few studies that cover periods of several decades. This limitation is crucial for understanding how glacier mass balances or runoff have been changing over time and how they could be altered under different climate change scenarios.

In the semi-arid Andes, glaciological studies that have examined glacier evolution over periods of several decades have primarily focused on the Maipo River basin (Masiokas and others, 2016; Farías-Barahona and others, 2019; Ayala and others, 2020). For example, Masiokas and others (2016) developed a model of surface mass balance for the Echaurren Norte Glacier. The North Echaurren Glacier, located in the Maipo River basin, is the glacier

with the most extensive mass balance record in the southern hemisphere, dating from 1971 to the present.

In recent years, the use of geodetic mass balances obtained from satellite sensors or photogrammetry has allowed for the calculation of changes in glacier volume and the estimation of mass balances through different assumptions about ice density. This methodology has significantly expanded the temporal and spatial coverage of glacier mass balance studies (Braithwaite & Hughes, 2020), moving from having only a few glaciers with geodetic balances or glaciological measurements available to nearly global coverage (Berthier and others, 2023). For example, ice elevation difference estimates generated by Hugonnet and others (2021) and Dusaillant and others (2020) using ASTER images have allowed different researchers to develop their work according to their specific needs (Barandun and others, 2022; Compagno and others, 2022; McCarthy and others, 2023; Li and others, 2023; Rounce and others, 2023). However, it is important to mention that there are differences between regional estimates from different research groups and available methods (Hugonnet and others, 2021; Berthier and others, 2023). The causes and consequences of these discrepancies are still not clear, although there are already initiatives focused on resolving them, such as the GlaMBIE project (Berthier and others, 2023).

Most techniques for obtaining geodetic mass balances, due to the sensors used, are only available after the year 2000 (Berthier and others, 2023, table 3). However, geodetic mass balances obtained from differences in digital elevation models generated through optical stereoscopic images present the possibility of conducting mass balance studies that span long periods of time, even from the 1960s. Nevertheless, this technique still faces various challenges, such as limitations in spatial coverage, subject to local studies, and potential problems due to cloud coverage, lack of contrast, especially in the accumulation area, and difficulty in finding stable terrains that act as control points (Berthier and others, 2023).

In the semi-arid Andes, geodetic mass balances are of special relevance, considering that mass balances through the glaciological method are limited due to logistical complications and associated costs (Farías-Barahona and others, 2020). Despite the significant opportunity they represent, there is still a limited number of studies that utilize them. For example, Barandun and others (2022) used the elevation changes from Hugonnet and others (2021) to calibrate the threshold temperature in an improved degree-day model. Similarly, Ayala and others (2020) used geodetic mass balances generated by Braun and others (2019) and extended by Farias-Barahona and others (2019) to calibrate glacier ice melt in the TOPKAPI-ETH model.

The Universidad Glacier (34°40'S, 70°20'W), located in the semi-arid Andes, at the head of the Tinguiririca River, is the largest glacier north of Patagonia, with an area of 26.3 km2 according to the Dirección General de Aguas (DGA, 2022). Due to its relatively large size compared to other glaciers in the region, the Universidad Glacier plays an important role as a water resource at the basin level. For example, during the summer of 2010/2011, the Universidad Glacier alone contributed 10-13% of the total flow of the Tinguiririca River basin in Bajo los Briones (Bravo and others, 2017). For comparison, all glaciers in the Maipo

River Basin contributed 55% of the summer runoff of the Maipo River between 2010-2015 (Ayala and others, 2020).

The present study aims to achieve two main objectives:

Investigation of the evolution of the Universidad Glacier, with a focus on analyzing trends and cycles of mass balances and glacier runoff. Additionally, considering the significance of the Universidad Glacier as a vital water resource, the study aims to quantify its contribution to the total runoff of the Tinguiririca Bajo los Briones Basin and analyze its evolution over time.

Assessment of the enhancements and discrepancies obtained by incorporating geodetic mass balances from diverse time periods characterized by distinct climatic conditions into the calibration process of a hydro-glaciological model.

The present study found a clear correlation between the Pacific Decadal Oscillation and the periods of glacier runoff and mass balance. Additionally, there has been an increasing trend in glacier runoff since the mid-1970s. The various calibration scenarios using different periods of geodetic mass balances exhibit consistent tendencies, with variations mainly in the accumulated values of mass balances.

2. Study domain and data

2.1. Study domain

The Universidad Glacier (34°40'S, 70°20'W) is situated in the semiarid Andes of central Chile, specifically in the Upper Tinguirirca Bajo Los Briones Basin. The nearest city to the glacier is San Fernando, located 55 km to the west and 120 km southwest of Santiago, the national capital (Figure 1). The regional climate exhibits a predominantly Mediterranean climate pattern, characterized by an average annual precipitation of 1600 mm. Most of the precipitation occurs during the winter months from May to September. The mean temperature in the region is around 6°C (Escanilla-Minchel and others, 2020). With an area of 26.3 km2 as of 2018 (DGA, 2022), the Universidad Glacier is the largest glacier in South America, north of the Patagonian Icefields. It spans an altitudinal range between 2482 and 4970 meters above sea level (m a.s.l) and has a predominant southeast orientation (DGA, 2022). The glacier comprises two sub-basins that serve as accumulation zones. These two accumulation zones merge downstream of the icefalls, forming the glacier tongue. The presence of debris on the glacier tongue is discontinuous, with the upper part exhibiting the formation of ogives (Wilson and others, 2016). While there is a greater presence of detritus near the end of the glacier, it does not form a homogeneous and continuous layer.

Due to its relatively large size compared to other glaciers in the central Andes, the Universidad Glacier plays an important role as a water resource at the basin level. For example, during the summer of 2010/2011, the Universidad Glacier alone contributed between 10-13% of the total flow of the Tinguiririca River basin in Bajo Los Briones (Bravo and other, 2017). For comparison, all glaciers in the Maipo River Basin contributed 55% of the summer runoff of the Maipo River between 2010-2015 (Ayala and others, 2015).

2.2. Data

2.2.1. Mass balances

To calibrate the Cold Region Hydrological Model (CRHM), we utilized the changes in glacier elevations calculated by Hugonnet and others (2021) and the mass balance data presented by Mahmoud and others (2022). Hugonnet and others (2021) utilized stereo images from the Advanced Spaceborne Thermal Emission and Reflection Radiometer (ASTER), ArcticDEM and Reference Elevation Model of Antartica (REMA) to derive surface elevation changes from the glaciers. They computed these changes for four five-year periods: 2000-2004, 2005-2009, 2010-2014, and 2015-2019.

On the other hand, Mahmoud and others (2022) calculated mass balance using geodetic methods based in historical photogrammetry. They utilized historical aerial photogrammetry data collected by the Aerial Photogrammetry Service (SAF) and Military Geographic Institute of Chile (IGM) in the years 1955, 1985 and 1997 to create Digitals Elevations Models, later co-registered with SRTM Digital Elevation Model. We incorporated their mass balance estimates for two periods: 1955-1985 and 1985-1997.

To validate the model, we utilized glaciological mass balances data from Kinnard and others (2018). Between 2012 and 2014, Kinnard and others (2018) conducted an extensive monitoring program for the Universidad Glacier. This program involved measuring mass balances for two consecutive years using the glaciological method, along with collecting meteorological data.

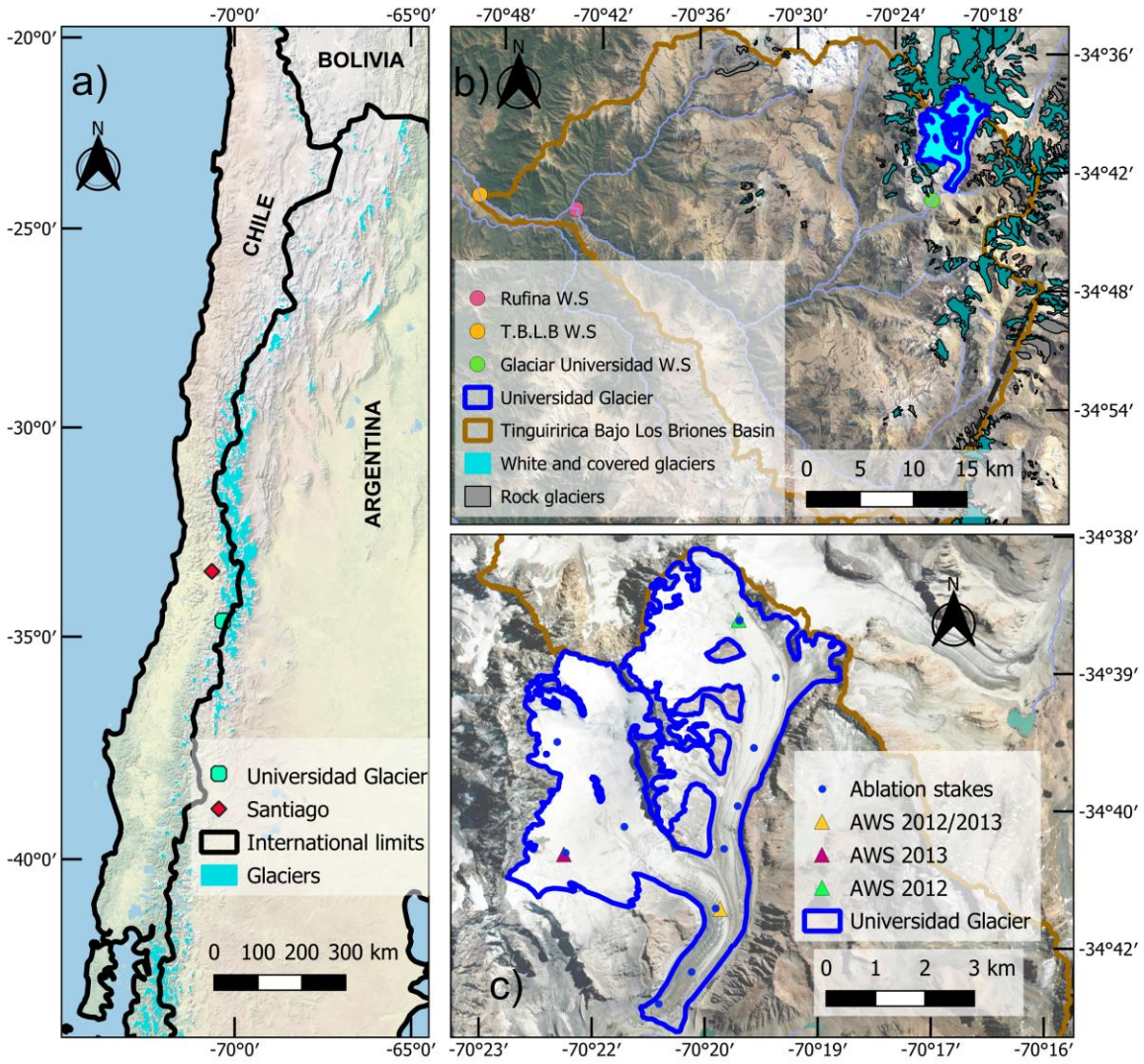

Figure 1. Panel a) Relative position of the Universidad glacier with respect to Santiago, capital of Chile. Panel b) Tinguiririca Bajo Los Briones basin and location of the gauging station. Also, the location of the Rufina (Rufina WS) and Universidad glacier (Glaciar Universidad WS) weather stations, used to calculate precipitation gradients. Panel c) Limits of the Universidad glacier (DGA, 2022), Automatic Weather Stations and ablations stakes of Kinnard and others (2018).

2.3. Meteorological data

In our study, we used the CR2MET meteorological dataset (Boisier and others, 2016) in conjunction with the hourly data of the ERA5 reanalysis product (Hersbach and others, 2020) to generate a bias-corrected ERA5-Land hourly time series for temperature and precipitation. The CR2MET dataset is grid-based and provides information on minimum, maximum, and mean daily temperatures, as well as accumulated daily precipitation for continental Chile. It was specifically developed for the National Water Balance Project (DGA, 2017) and covers the period from 1979 to 2016, with a horizontal and vertical resolution of 0.05°.

CR2MET was created using statistical downscaling techniques that incorporate the ERA5 reanalysis product and topographic predictors. The daily precipitation data is obtained

through multiple linear regressions that are calibrated against quality-controlled precipitation records. Maximum and minimum temperatures are derived using a similar procedure, utilizing near-surface temperature data from ERA5-Interim and land surface temperature data from MODIS.

To determine the temperature gradients, we relied on data collected from two Automatic Weather Stations (AWS) (Figure 2) installed during the campaign conducted by Kinnard and others, (2018). These AWS stations capture various meteorological variables, including air temperature, pressure, humidity, wind speed, incoming and outgoing shortwave and longwave radiation, and changes in surface height. The AWS station located in the lower part of the glacier, situated at an elevation of 2790 m a.s.l, operated continuously from November 25, 2012, to April 24, 2014. As for the AWS station in the upper part of the glacier, it was relocated during the ablation seasons. Initially, it was positioned in the east accumulation zone at an elevation of 3629 m a.s.l, and recorded data between November 25, 2012, and May 15, 2013. Subsequently, it was moved to the west accumulation zone at an elevation of 3724 m a.s.l, where it operated from October 23, 2013, to April 29, 2014 (Figure 1b).

Table 1 shows a summary of the different sources used.

Table 1: Sources and temporal coverage of data used.

Source	Temporal cover	Variables
CR2met gridded product (Boisier and others, 2016)	1979-2016	Two meters daily mean, maximum and minimum temperature (°C).
ERA5 Land (Hersbach and others, 2020)	1950-present	Two meters hourly temperature (°C). Total precipitation (mm)
Automatic Weathers Stations (Kinnard and others, 2018)	2012-2014	Relative Humidity (%); Albedo (-); Wind speed (m/s); Two meters temperature (°C); short and longwave incident radiation (w/m^2).
Geodetic mass balances (Mahmoud and others, 2022)	1955-2000	Geodetic mass balances (m. $w.e.a^{-1}$)
Difference in ice elevation (Hugonnet and others, 2021)	2000-2020	Difference in the ice surface elevation (m a^{-1})

3. Methodology

3.1. Meteorology

To force the hydro-glaciological model, three-hourly series of temperature, precipitation, wind speed and relative humidity must be generated.

To obtain the temperature and precipitation series, a bias-corrected ERA5-Land dataset is generated. The first step involved in generating the bias-corrected ERA5-Land dataset is interpolating ERA5-Land to match the spatial resolution of CR2MET by applying an inverse distance method. Next, we applied the Multivariate Quantile Mapping Bias Correction (MBCn) technique (Cannon, 2018) to correct the daily aggregated ERA5-Land data for the period 1955-2020. The variables used for the correction were minimum and maximum daily temperature, and daily precipitation of the CR2met and ERA5-Land. The bias correction process was performed twice for the same historical period (1979-2015) but with different predicted periods: 1955-1979 and 2015-2019.

We chose the MBCn method for its multivariate nature, enabling the simultaneous correction of precipitation and temperature. This approach preserves the relationship between these variables, leading to a more accurate representation of snowfall compared to univariate methods (Eum and others, 2020). Moreover, the simplicity of implementing the MBCn method through the R package MBC (Cannon, 2020) made it a suitable choice for our analysis.

After the daily series underwent bias correction, we further disaggregated them into three-hourly time steps by utilizing the hourly distribution of the ERA5-Land data. Is important to note that this procedure was necessary because the CR2MET dataset did not cover the entire study period.

Due to the limited spatial coverage of the product, where only a few pixels cover the entire glacier, we employed an extrapolation method to estimate temperature, precipitation, and relative humidity values for each Hydrologic Response Unit (HRU) within our model. We utilized altitudinal gradients to extrapolate the data from the pixel representing the tongue of the glacier and part of the accumulation zones to the other HRUs.

To determine the air temperature gradients, we calculated the hourly differences between the upper and lower AWS. Subsequently, the mean of these differences was employed as the gradient in the model. Three linear elevation gradients were derived. One gradient was determined for the easter accumulation zone of the glacier, using the temperature data from December 2012 to May 2013 ablation period. Another gradient was calculated for the western accumulation zone using temperature data from November 2013 to April 2014.

The calculated temperature gradient for the eastern part of the glacier was 5.5°C km^{-1}, with a standard deviation of 1.0°C km^{-1}. This calculated gradient for the eastern zone aligns with the average 6.0°C km^{-1} hourly gradient calculated by Bravo and others (2017) using two AWS located in similar positions during the period between December 2009 and March

2010. For the western part of the glacier, we computed a gradient of 7.6°C km-1 with a standard deviation of 0.9 °C km-1. The western gradient is stronger than the register for the easter zone, and this difference may be attributed to the varying exposition of the two zones. Figure 2a illustrates the predominant exposition of the glacier, slope, elevation, and the spatial discretization of the model. While in the easter zone of the glacier, where the two AWS were placed to calculate the eastern gradient, the aspect is mainly to the west, the western part of the glacier has a predominant north orientation. None of the hourly gradients used to calculate our mean gradient show periods of inversion.

To distribute precipitation on the glacier, we utilized a logarithmic gradient (Equation 1) derived from the precipitation data obtained from three weather stations operated by the DGA. These weather stations, namely "Río Tinguiririca Bajo Los Briones," "La Rufina," and "Glaciar Universidad," were situated at elevations of 560 m.a.s.l, 743 m.a.s.l, and 2429 m.a.s.l, respectively, as depicted in the Figure 1. The logarithmic gradient was calculated using the precipitation measurements recorded between July 2018 and April 2020.

$$P_{HRU} = (0.33 \cdot \ln(z) - 1.6) \cdot P_{ERA.BC} \quad (1)$$

Where P_{HRU} is the precipitation in the HRU; *z* is the elevation of the HRU and $P_{ERA.BC}$ is the precipitation at the centroid of the ERA5-Land bias corrected precipitation time series. The calculated gradient is in the range of that calculated in Ragettli and others (2014) for the Andean Valleys in central Andes basins.

The wind speed and relative humidity series for the hydro-glaciological model were constructed using synthetic series based on the records from the AWS located in the lower part of the glacier. The AWS records, which were originally aggregated at a three-hourly scale, were used as the basis for generating the synthetic series.

The series were calculated by considering an additive model with three components: seasonal, trend, and random. A different series was calculated for each month. The daily cycle was considered as the seasonal component of the series, capturing the variation in wind speed and relative humidity throughout the day.

To distribute relative humidity across the glacier, an altitudinal gradient was calculated using the same procedure as for temperature. For the eastern part of the glacier, the calculated altitudinal gradient was -0.01% km^{-1}. For the western part of the glacier, the gradient was -0.0065% km^{-1}.

Regarding wind speed, it was found that there was no significant relationship between the upper and lower AWS that would allow for the calculation of a gradient. Therefore, the same wind speed value obtained from the lower AWS was used for the entire glacier.

3.2. Universidad Glacier hydro-glaciological model

We implemented a semi-distributed hydro-glaciological model of the Universidad Glacier using the Cold Region Hydrological Model (CRHM) platform, as described by Pomeroy

(2007). The model structure for the glacial watershed was based on the framework presented in the studies by Pradhananga & Pomeroy (2020; 2022).

CRHM is a physically based model that allows for the simulation of various processes related to snow accumulation, ablation, and runoff. It achieves this by integrating different modules that represent these processes. Originally, CRHM did not have a glacier module, but was developed and coupled by Pradhananga & Pomeroy (2022) and named CRHM-glacier.

CRHM is a semi-distributed model, which means that it divides the study area into different HRUs. This approach enables a more detailed representation of the spatial variability within the watershed and helps reduce computational time.

3.2.1. Hydrological Response Units

Hydrologic Response Units for the Universidad Glacier were defined based on topographic attributes and glacier boundaries. The glacier contour used was obtained from the Public Glacier Inventory (DGA, 2022) and corresponds to the boundaries of the Universidad Glacier for 2018. The elevation data was obtained from ASTER DEM (ASTER Science Team, 2019). Using the r.slope.aspect command in QGIS software, the aspect and slope were derived from the ASTER DEM. The elevation was divided into bands of 100 meters each. The slope was reclassified into three classes: 0-25°, 25-60°, and 60-90° (Marcoleta, 2019). The aspect was categorized into four main orientations: north (0-45° & 315-360°), east (45-135°), south (135-225°), and west (225-315°). Figure 2 illustrates the topographic attributes of the glacier and the created HRUs. We obtained 55 HRU with an average size of 0.54 km^2.

3.2.2. Model Structure

Figure 3 illustrates the general structure of the CRHM model for the Universidad Glacier, highlighting the interconnectedness of the main processes. The model follows a sequential flow of processes. Initially, meteorological data undergo preprocessing to ensure their compatibility with the model requirements. Subsequently, the calculation of radiation fluxes and, if applicable, canopy interception of energy and mass fluxes. The model then proceeds to compute snow accumulation and transport processes. Following this, the melting of snow and/or increase of glacial ice are determined. Finally, the model calculates the fluxes of infiltration, evaporation, and runoff for the entire basin.

The melting processes in the CRHM model are treated separately for the snow and glacier components. Snowmelt for both glacier and non-glacier HRUs is calculated using the SNOBAL module (Marks and others, 1999). SNOBAL is an energy and mass balance model that divides the snowpack into two layers: an active layer and a lower deep snowpack, as described by Pradhananga & Pomeroy (2022). Through SNOBAL, the model computes the mass and energy fluxes between the atmosphere and the active layer, as well as between the active layer and the lower layer, to determine the energy available for melting.

The redistribution of snow between different HRUs is considered through two mechanisms: gravitational transport and blowing snow. Gravitational transport is based on the work of

Bernhard & Schulz (2010) and is implemented in the SWESlope module. The Prairie Blowing Snow Module (PBSM) (Pomeroy, 1993; Pomeroy & Li, 2000) calculates blowing snow transport and accounts for the sublimation that occurs during the blowing snow process.

In the CRHM-glacier model, ice melt and firn are calculated using an energy balance approach. The model considers a single isothermal layer of ice and all internal energy changes are used for ice melting. The firn is divided into several layers depending on its density, but for the purpose of energy changes, it is considered as one isothermal layer and similarly as for ice, all energy changes are used for firn melting (Pradhananga & Pomeroy, 2022).

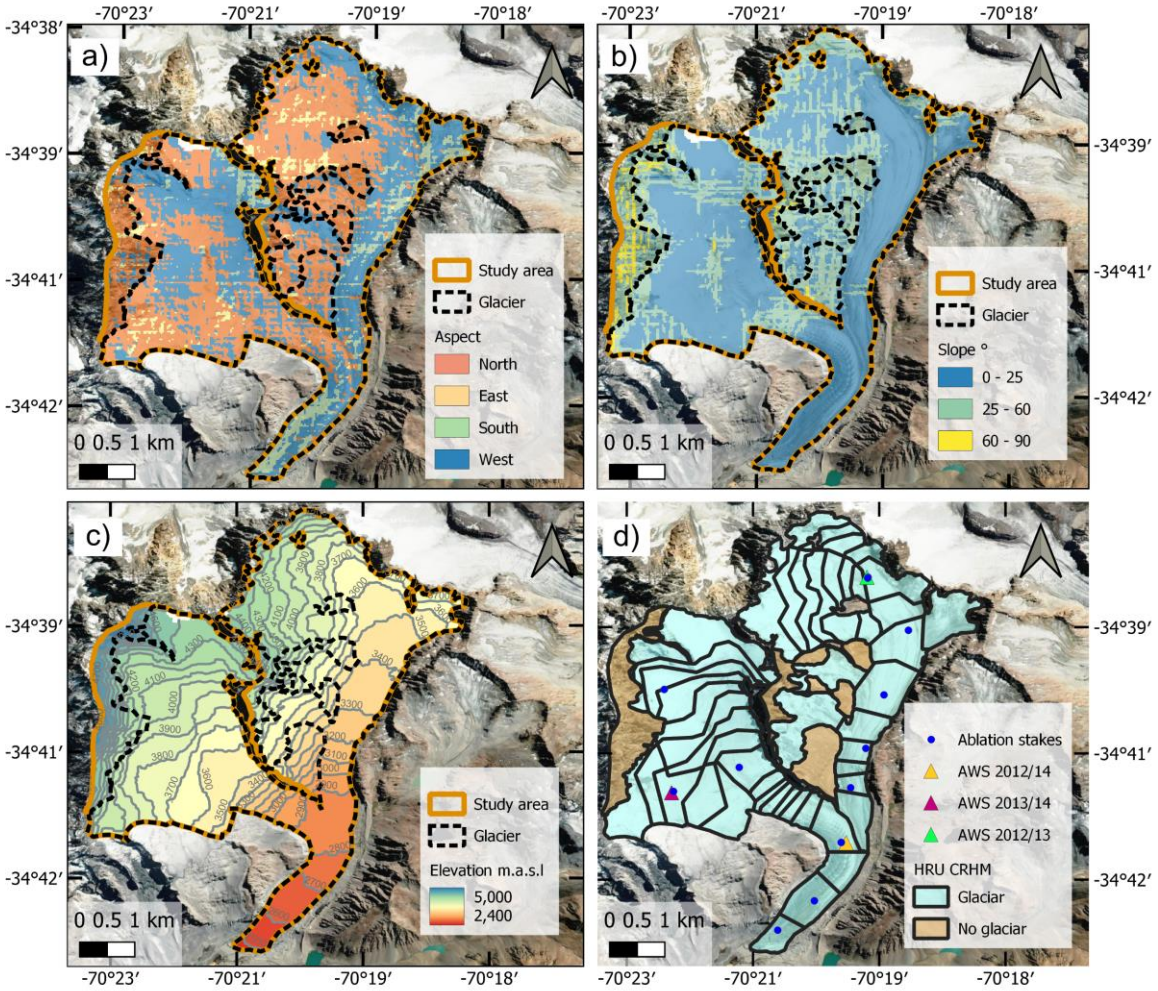

Figure 2: Topographic attributes for HRU discretization. Top left panel: Aspect discretization. Top right panel: Slope discretization. Bottom left panel: Altitudinal. Bottom right panel: glaciers and non-glaciers HRU's of the CRHM model for the Universidad glacier. The blue dots are the ablation stakes of Kinnard and others (2018) while the triangles are the AWS of the same study.

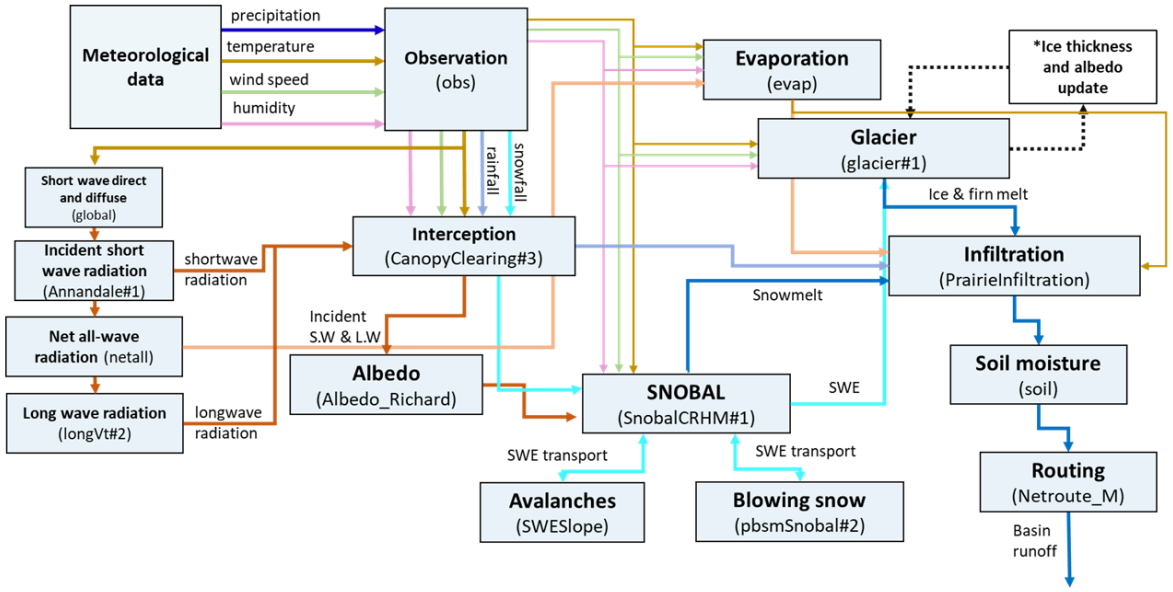

Figure 3: CRHM modular structure. The lines indicate the meteorological variables, mass, and energetic fluxes between the modules.

Additionally, the CRHM-glacier model incorporates the gradual integration of firn into glacier ice through a densification process. As the ablation season progresses, the remaining snow is transformed into firn. The firn undergoes changes in density using a multilayer model based on Herron and Langway (1980). The density changes depend on the pressure exerted by the upper layers of snow and firn until it eventually becomes part of the glacier ice.

To calculate R_s, the first step is to determine the extraterrestrial radiation R_a (MJ m^{-2} d^{-1}) for a given latitude and day of the year. This calculation follows the method described by Garnier & Omura (1970). The obtained R_a is then corrected for atmospheric transmissivity (T_t) using the equation shown in Equation 2 and 3. The correction for atmospheric transmissivity is based on the approach proposed by Annandale & Jovanovic (2002).

$$R_S = R_a \cdot T_t \tag{2}$$

$$T_t = k_{rs} \cdot (1 + 2.7 \cdot 10^{-5} \cdot Z) \cdot (T_{max} - T_{min})^{0.5} \tag{3}$$

Where Z m a.s.l is the elevation, T_{max} and T_{min} °C are the maximum and minimum daily temperature, and k_{rs} is an adjustment coefficient, 0.16 for interior regions and 0.19 for coastal regions. We obtained an underestimation of the modeled incident shortwave radiation (Rs) when using the recommended factor of 0.16 for an interior region. However, a better representation was obtained by using a factor of 0.2, which is slightly higher than the recommended value for coastal regions. The incident shortwave radiation is also adjusted for slope and aspect.

The calculation of longwave radiation is performed using the incident shortwave radiation, air temperature, and relative humidity using the algorithm developed by Sicart and others (2006).

In the CRHM-glacier model, the treatment of albedo differs for snow albedo and firn/ice albedo.

For snow albedo, the model follows the evolution presented in Verseghy (2012). The snow albedo (α_t) exhibits a linear decay for cold snow, while melting snow has an empirical exponential decay function as described in Equation 4. This representation captures the changes in albedo as snow undergoes melt processes.

$$\alpha_t \begin{cases} \alpha_{t-1} - \dfrac{\Delta t}{a_1}, \text{cold snow} \\ (\alpha_{t-1} - \alpha_{min}) \cdot e^{-\frac{\Delta t}{a_2}} + \alpha_{min}, \text{melting snow} \end{cases} \tag{4}$$

Furthermore, the snow albedo is refreshed based on the magnitude of snowfall, as shown in Equation 5.

$$\alpha_t = \alpha_{t-1} + (\alpha_{max} - \alpha_{t-1}) \cdot \left(\frac{s_f}{s_{min}}\right) \tag{5}$$

Where α_{t-1} and α_t is the albedo for the previous and actual time step respectively. α_{max} and α_{min} is the maximum albedo of fresh snow and minimum albedo of the aged snow. s_f is the amount of snowfall in the time step, and s_{min} is the minimum amount of snowfall required in the time step to refresh the albedo to α_{max}.

The value of α_{max} is determined based on daily snow albedo data derived from the MODIS products Terra Snow Cover Daily L3 Global 500m (MOD10A1) (Hall & Riggs, 2021) and Aqua Snow Cover Daily L3 Global 500m (MYD10A1) (Hall & Riggs, 2021). By averaging the annual maximum snow albedo over the glacier for the period 2000-2020, we obtained a value of 0.90. This value is consistent with the AWS observations reported by Kinnard and others (2018).

The α_{min} is derived from the albedo grids calculated in the study conducted by Shaw and others (2020). These grids can be accessed through a Zenodo repository (http://doi.org/10.5281/zenodo.3937676.). Shaw and others (2020) examined the glacier albedo of various glaciers in the central Chilean Andes (33-34°S) using late summer Landsat scenes between the years 1986-2020, revealing a negative albedo trend. They manually selected optimal scenes with minimal snow cover at the end of each summer for the years from 1989 to 2020 and classified the bare ice and snow cover zones for each glacier. Albedo grids specifically for the Universidad glacier are available for the period between 1991 to 2020.

To calculate the minimum albedo for snow-covered areas, we assumed that the remaining snow was in the melting process and had reached its minimum value for the season. We averaged the annual minimum values, resulting in a minimum snow albedo of 0.35. This value is consistent with the AWS observation reported by Kinnard and others (2018) and is similar to the March monthly mean albedo calculated for the Central Andes (Malmros and others, 2018).

The decay parameter a_1 is determined from linear regressions of albedo decay calculated in the study of Comte (2017), using winter snowfall data from the Valle Nevado cryosphere station (33°21'S, 70°14'W, 3030 m a.s.l.). We obtained a value of 34.72 d for a_1.

For the parameter a_2, we adopted a value of 1.39 d, which is the same as the study conducted by Jara and others (2021) for an Andean Basin (4320 m a.s.l, 28°2'S, 69°5'W). Furthermore, we set the value of smin to 1 mm, following the approach employed by Jara and others (2021).

In the original CRHM-glacier model, the ice and firn albedo were fixed parameters throughout the entire simulation period. However, considering that the Universidad Glacier has experienced a decreasing trend in ice albedo since 1990 at a rate of -0.014 per decade (Shaw and others, 2020), and acknowledging the importance of incident radiation as the main driver of ablation (Bravo and others, 2017; Kinnard and others, 2018), we made modifications to account for these changes.

To adjust the ice albedo values on an annual basis, we utilized the ice albedo grid data from Shaw and others (2020), which was also used for determining the minimum snow albedo. For each glacier-HRU, we calculated the mean ice albedo for each year between 1991 and 2020 and fitted a linear decay trend. For HRUs located above the equilibrium altitudinal line (ELA), we considered the lowest albedo decay rate.

For years prior to 1990, we used fixed ice albedo values obtained from the 1991 ice albedo grid provided by Shaw and others (2020).

Regarding the firn albedo, we set it to 0.35 to maintain coherence with the minimum snow albedo (α_{min}) value, and this value remains constant throughout the entire model period.

In the CRHM-glacier model, the simulation of ice flow dynamics is not included (Pradhananga & Pomeroy, 2022), which can pose challenges, especially in large-scale simulations. Without considering ice flow, the model may overlook the redistribution of ice from the accumulation zone to the ablation zone. This oversight can lead to unrealistic changes in glacier geometry (Huss and others, 2010) and potentially result in the disappearance of the lowest HRUs.

To distribute the ice thickness and avoid unrealistic disappearance of the lowest HRUs and exaggerated mass gain in the higher HRUs, we implemented the widely used Δh parametrization (Huss and others, 2010). The Δh parametrization is an empirical function specific to glaciers that relates changes in glacier elevation to the elevation of the glacier surface. In our study, we obtained the elevation change data from Hugonnet and others

(2021) for the period 2000-2019. The elevation bands used in the parametrization correspond to the same intervals of 100 m that were utilized for generating the HRUs (see Figure 2).

CRHM does not account for changes in the geometry or area of the glacier. In our study, we assume that maintaining a constant area for the Universidad glacier is appropriate for modeling purposes. This assumption is supported by the fact that the glacier experienced a relatively modest area loss of only 6% between 1945 and 2011 (DGA, 2011).

3.3. Model Calibration

To calibrate the Universidad glacier model, we performed a sensitive analysis using the Distributed Evaluation of Local Sensitivity Analysis method (DELSA) (Rakovec, 2014). This analysis aimed to identify the three most sensitive parameters among those listed in Table 2. DELSA employs "local" derivate-based methods to obtain the sensitivity of the sensitivity of the parameters based on the response in the gradient of the model output or a performance index. The sensitivity of the parameters is assessed across the parameter space by selecting different points using a Latin hypercube. We opted for the DELSA method due to its capability to evaluate the sensitivity of parameters across the parameter space with relatively low computational cost, along with its relevance to the other parameters under investigation. The parameters selected to conduct the sensitivity analysis were selected as calibration candidates due to their potential impacts in glacier accumulation and ablation process.

To study the differences between models calibrated with different mass balances periods, we calibrated two models. The first model was calibrated using mass balances from 2000 to 2020, generated from the work of Hugonnet and others (2021). This period is characterized by higher glacier mass loss, elevated temperatures, and the occurrence of the megadrought since 2010. The second model was calibrated using mass balances from 1955 to 2020, incorporating geodetic mass balances from Hazem and others (2022) and the work of Hugonnet and others (2021). The period from 1955 to 2000 covers greater hydroclimatic variability, including some shorter drought periods compared to the current megadrought, along with an increasing temperature trend (Burger and others, 2018). Figure 4a shows the value per period of the geodetic mass balances per period together with the annual precipitation and temperature series. The models were calibrated using the Shuffled Complex Evolution Global Optimization Method (SCE) (Duan and others, 1993) implemented in the Rtop package. SCE is a search algorithm that allows to find the global optimal by the combination of the SIMPLEX method, random search, and competitive evolution to find the global optimum by minimizing an objective function. The objective function aimed to reduce the value of the evaluation metric Root Mean Square Error (RMSE) of the mass balance for each period (Equation 6), considering the geodetic mass balances as reference.

$$\text{RMSE M.B} = \sqrt{\frac{1}{m}\sum_{j=i}^{m}(\Delta h_{ref\,i} - \Delta h_{sim\,i})} \quad (6)$$

$\Delta h_{ref,i}$ is the geodetic mass balance of the period, $\Delta h_{sim\ i}$ is the mass balance calculated by the model.

3.3.1. Identification of periods and trends

To examine the different periods of evolution of the Universidad glacier, we applied a methodology inspired by Faely and Sweeney (2005) to identify change points. However, in this study, we directly applied the change point analysis to various glaciological variables of interest, including mass balance, runoff, and equilibrium altitudinal line.

To visually identify the points where the trends in the cumulative sum of deviations (CUSUMs) series changed, we conducted an analysis of the CUSUMs in the annual time series. Additionally, we employed Pettitt's non-parametric test (Pettitt, 1979) to confirm these change points. The equation used to perform the CUSUMs analysis is shown in Equation 7.

$$S_i = \sum_{i=n} (x_i - k) \tag{7}$$

Where S_i is the CUSUMs analysis, x_i represents the yearly value of the variable of interest, and k is the average of the historical series of the variable.

Furthermore, we employed the Mann-Kendall test to determine the statistical significance of the trends observed in the annual time series.

Table 2: Candidate parameters evaluated in the DELSA analysis with their respective ranges for calibration.

Parameter	Description	Range	CRHM module	Comment
S_{min}	Minimum snowfall to refresh snow albedo	0.5~15 (mm)	Albedo	We use the 50% of Jara and others (2021) as lower limit and a 50% more than the value used in Essery (2004)
α_{min}	Minimum albedo for aged snow	0.3~0.6 (-)	Albedo	The lower limit corresponds to the minimum value for old debris wet snow. The upper limits used is the maximum value for old clean wet snow (Cuffey & Patterson, 2010)
α_{max}	Maximum albedo for fresh snow	0.75~0.98 (-)	Albedo	Values for fresh snow as described in Cuffey and Patterson (2010)
firn_Albedo	Firn albedo	0.40~0.70 (-)	Glacier	Values for firn albedo as described in Cuffey and Patterson (2010)
tmax_allrain	Precipitation is all rain when the temperature is greater or equal to this value	1~4(°C)	Observations	The lower limit corresponds to the conditional snow frequency of 50% for a pressure of 770 hPa. The upper limit is the temperature corresponds to the conditional snow frequency of 5%. (Figure 5a. Behrangi and other, 2018)
tmax_allsnow	Precipitation is all snow when the temperature is less or equal to this value	-2 ~1 (°C)	Observations	The lower limit corresponds to the conditional snow frequency over land of 95% for a pressure of 770 hPa. (Figure 5a. Behrangi and others, 2018)

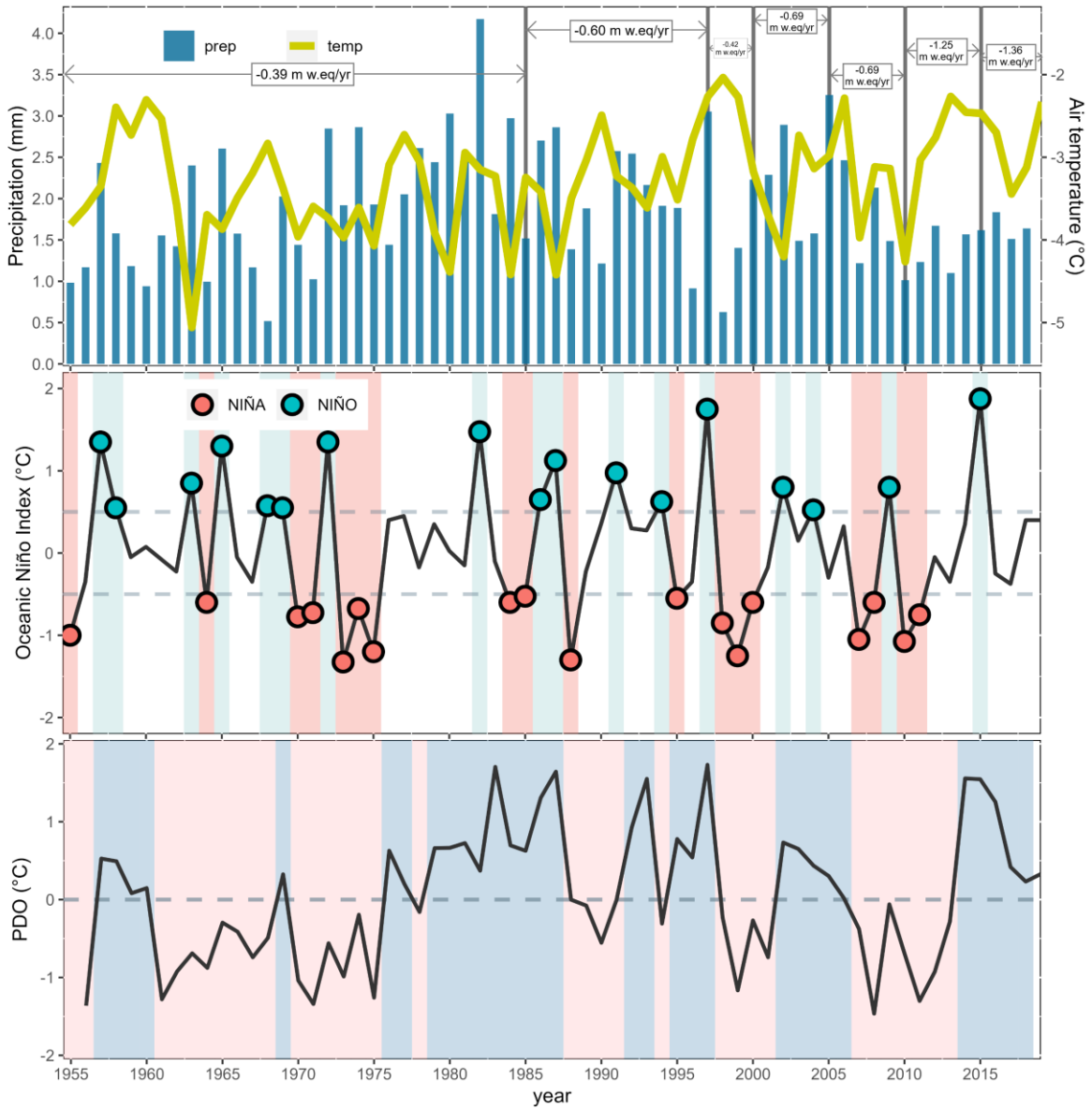

Figure 4: a) Average annual temperatures, average annual precipitation over the glacier. The arrows and vertical lines indicate the average mass balance for the university glacier in the delimited periods. The sources are in Table 1. b) Annual series of the Oceanic Niño Index (ONI), the light blue bands correspond to years NIÑO while the red bands correspond to years NIÑA. c) Pacific Decadal Oscillation Index.

4. Results

4.1. Parameter sensitivity and Calibration

Figure 5 illustrates the first-order sensitivity of the DELSA analysis applied to the uncalibrated CRHM model of the Universidad glacier. The two most sensitive parameters, α_{max} and S_{min}, are associated with the snow albedo, while the last parameter selected for calibration, tmax_allsnow, pertains to the module obs that manages the meteorological forcings in CRHM.

The values of the calibrated parameters are presented in Table 3. Both calibrated models exhibit similar values for α_{min}, indicating convergence in this parameter. The main difference

between the models lies in the value of the S_{min} parameter. The cext model, which is the CRHM model of the Universidad glacier calibrated using the mass balances from Mahmoud and others (2022) for the years 1955-2000 and Hugonnet and others (2021) for 2000-2020, converges to a lower value of S_{min}. A lower value of S_{min} means that a smaller amount of snow is required to completely refresh the albedo, reducing the energy absorbed by the snowpack allowing for a longer duration, subsequently reducing the time in which the ice is exposed, causing a gently ablation.

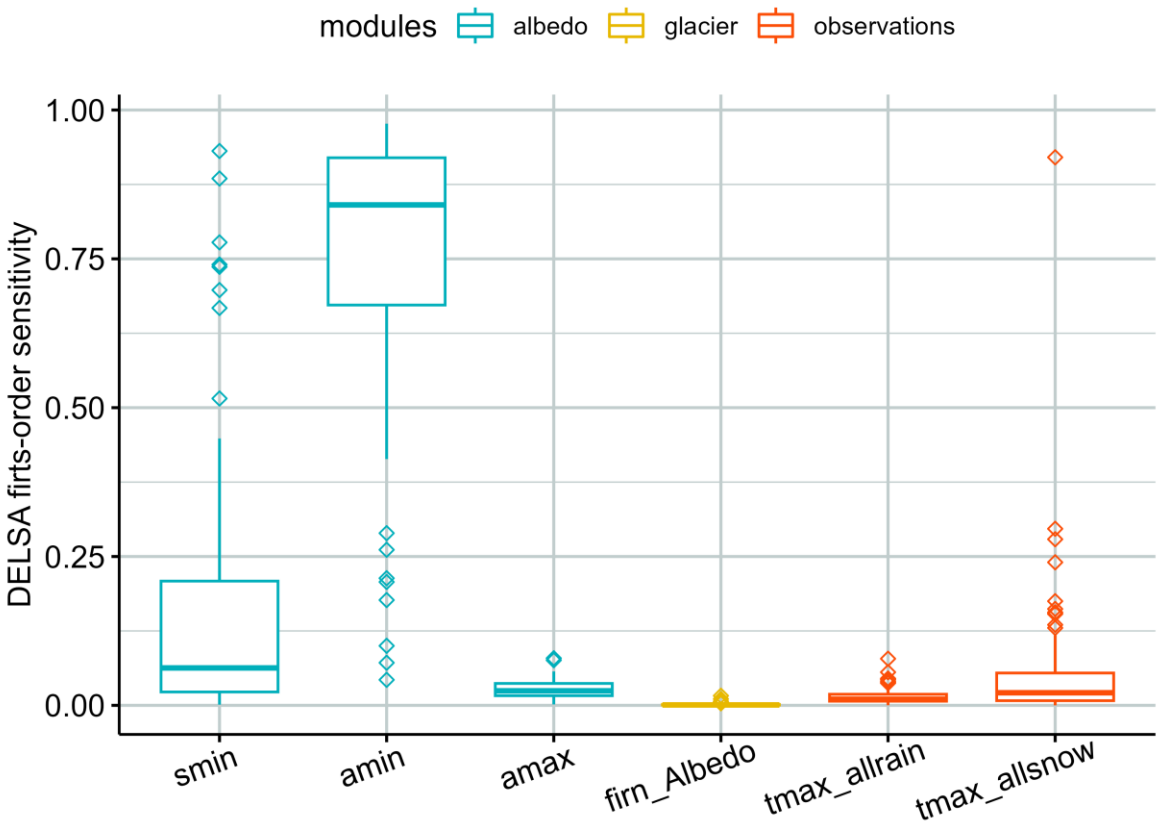

Figure 5: DELSA first-order sensitivity of the selected CRHM parameters. DELSA analysis was conducted with a sample size of n = 100.

Table 3: The calibrated models, along with their corresponding parameter values and sources of calibration. The 'Uncalibrated'(unc) model represents the model in its original state, where all parameters are obtained as described in the methodology section. The 'Calibrated Recent Period' (crec) model is calibrated using elevation differences obtained from Hugonnet and others (2021), which were converted into mass balances considering an ice density of 850 kg/m³ and the glacier outlines of 2018. The 'Calibrated Extended Period' (cext) model is calibrated using data from Hugonnet and others (2021) and mass balances for the years 1955-1997 from Mahmoud and others (2022).

Model	**Periods of G.M. used for calibration**	**Source GMB**	**amin (-)**	**smin (-)**	**Tmax_allsnow (°C)**
Uncalibrated (unc)	No calibration	-	0.35	1	-1
Calibrate recent periods (crec)	2000-2004; 2005- 2009; 2010-2014; 2015-2019	Hugonnet and others (2021)	0.46	3.4	0.39
Calibrate extended period (cext)	1955-1985; 1985-1997; 1997-2000; 2000-2004; 2005-2009; 2010-2014; 2015-2019	Hugonett and others (2021) Mahmoud and others (2022	0.45	0.6	0.27

4.2. Model evaluation

To evaluate the models' ability to accurately represent the energy and mass balances, we compared the modeled daily mean albedo and height of the snowpack with the AWS records shown in Figure 1. The results of various evaluation metrics for albedo and snowpack height are presented in Tables 4 and 5, respectively.

Figure 6 displays the time series for the AWS located in the ablation zone, which has the longest record covering both the accumulation and ablation seasons. For this station, all three models perform well in terms of albedo (WBI > 0.87, RMSE < 0.15, and MBE < 0.05) and snowpack height (WBI > 0.95, PBIAS < 18%, and MBE < 0.12). The models successfully capture the albedo variability and snowpack height during the accumulation period, with Pearson correlation values exceeding 0.97. However, their performance decreases during the ablation period (after 2013/10/1). It is observed that the modeled albedo experiences a rapid decay at the beginning of October, leading to a swift snowmelt. This accelerated decay in the snowpack is halted by snowfalls at beginning of November, which are not sufficient to increase accumulation but significantly impact the albedo of the models, allowing for a complete refreshment of the albedo and thus delaying the complete disappearance of the snowpack. Despite these shortcomings in the simulation, the maximum accumulation differs by less than 40 cm of the snowpack, and there is only a one-week difference in the total disappearance of the snowpack.

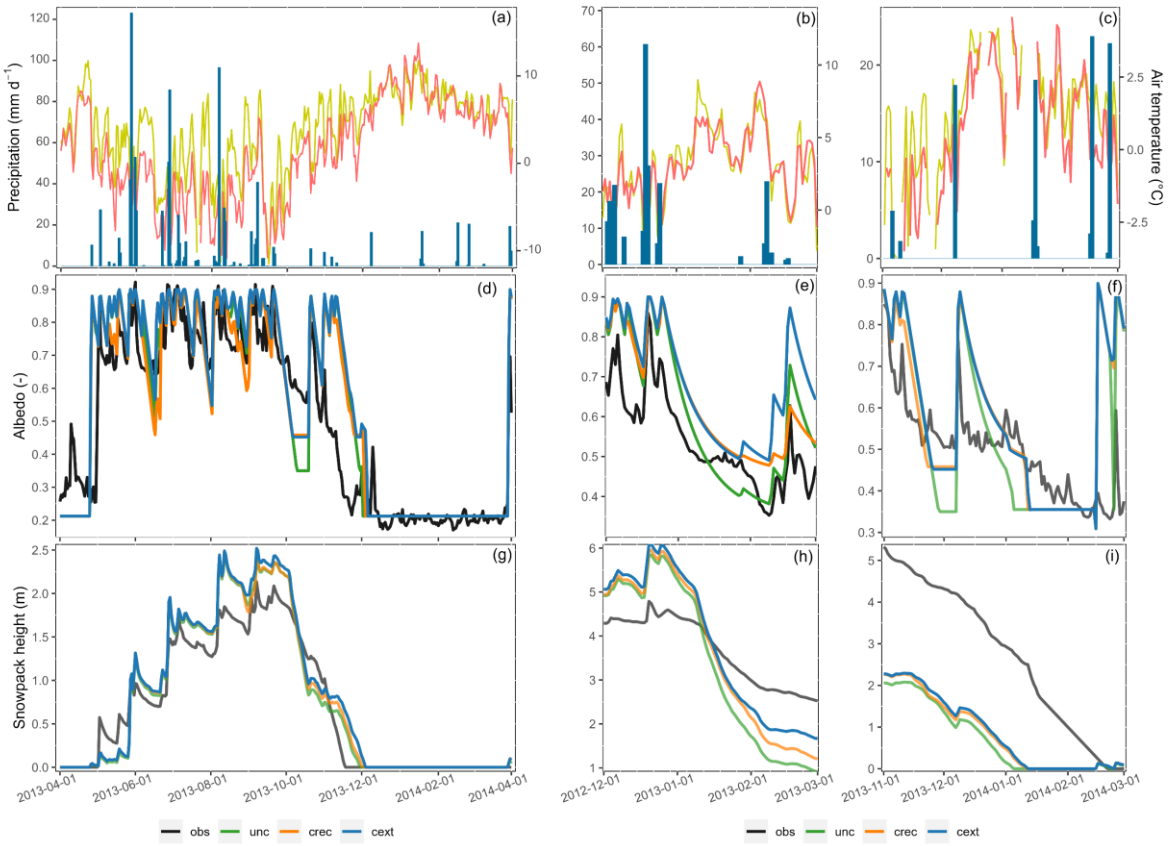

Figure 6: The lefts panels correspond to the measurements from the AWS located in the tongue of the glacier, the middle panels are from the AWS placed in the northeast in the 2012/2013 zone, and the right panels are from the AWS located in the northwest zone for the 2013/2014 summer, the positions are show in the Figure 1c. (a), (b),(c) Daily precipitation, In situ recorded mean temperature (yellow line) and mean temperature from ERA5-land corrected (red line). (d), (e), (f) Simulated and observed albedo for the CHRM models and in-situ record. (g), (h), (j) simulated and recorded snowpack height.

For the 2012/2013 ablation season depicted in the b panel of Figure 6, the calibrated models demonstrate favorable performance in albedo simulation, maintaining high values of temporal correlation (r-pearson > 0.81) and variability (Vxy > 0.92). However, they exhibit a positive bias, except for the uncalibrated model, which, owing to its low minimum albedo value, undergoes an exaggerated decay, resulting in an underestimation of albedo for certain weeks. Regarding the snowpack, there is good temporal correlation (r-pearson > 0.99), simulating a period of stability until the first week of January, followed by a rapid decline caused by a temperature increase, succeeded by a smoother decline in February. The fact that the worst performing metric in the Wang-Bovik Index is the difference in variance (Vxy < 0.77), along with high RMSE values (RMSE > 0.89 m, Table 4) shows that all models tend to overestimate the variability of the snowpack.

The poorest results are obtained when comparing the modeled values with the AWS records from the western region for the 2013/2014 ablation season (Figure 6 c). The accumulated observed values are more than twice the modeled values (Pbias < -68%), resulting in almost a two-month difference in snowpack disappearance between the modeled and observed

values. Despite that, the models experience similar ablations rates as the observed one. The cext model, between the middle of November, when the simulated snowpack enters the phase of mature snow, and the complete disappearance of the snowpack at middle of January, the snowpack decreases at a rate of 3.9 cm d^{-1}. The observed snowpack, which shows a continuous decay between the middle of November and its complete disappearance near the end of February, experiences a decrease of 4.6 cm d^{-1}. Due to the similar behavior of snowmelt between the models and the observed, the difference in the snowpack height is mainly attributed to the total accumulation. These difficulties in reproducing the precipitation gradient present in the glacier or the failure to capture local distribution mechanism such as avalanches or blowing snow favoring greater accumulation at the AWS point. It is important to consider that the AWS registers correspond to punctual measurements, highly sensitive to local topography, and may not necessarily be representative of the average behavior of the HRU in which the model is discretized.

Table 4: Comparison between in-situ measurements and modeled albedo by the differents study cases. WBI (-): Wang-Bovik Index; MBE (m): Mean Bias Error (m); RMSE (m): Root Mean Square Error; Mxy (-) : Difference in means; xy (-) : Difference in variance; Vxy (-): Pearson correlation. Mxy, Vxy and Rxy are part of WBI.

	AWS 2012/2014			AWS 2012/2013			AWS 2013/2014		
Metric	unc	crec	cext	unc	crec	cext	unc	crec	cext
WBI	0.87	0.88	0.86	0.79	0.83	0.68	0.44	0.46	0.46
MBE	0.04	0.03	0.06	0.07	0.10	0.15	0.04	0.06	0.07
RMSE	0.15	0.13	0.15	0.11	0.12	0.17	0.17	0.17	0.18
m_{xy}	0.99	1.00	0.99	0.95	0.91	0.85	0.98	0.96	0.95
v_{xy}	0.99	1.00	0.99	0.92	0.98	0.98	0.88	0.90	0.89
R_{xy}	0.88	0.88	0.88	0.90	0.93	0.81	0.52	0.53	0.55

Table 5: Comparison between in-situ measurements and modeled snowpack height by the differents study cases. WBI (-): Wang-Bovik Index; MBE (m): Mean Bias Error; RMSE (m): Root Mean Square Error; Mxy (-) : Difference in means; Vxy (-) : Difference in variance; Rxy (-): Pearson correlation. Mxy, Vxy and Rxy are part of WBI.

	AWS 2012/2014			AWS 2012/2013			AWS 2013/2014		
Metric	unc	crec	cext	unc	crec	cext	unc	crec	cext
NSE	0.90	0.90	0.88	-1.21	-0.61	-0.36	-0.18	-0.04	0.01
Pbias	10.70	13.40	17.40	-8.50	-1.70	-0.90	-73.80	-69.7	-68.1
WBI	0.96	0.96	0.95	0.70	0.74	0.76	0.30	0.37	0.40
MBE	0.07	0.09	0.12	-0.31	-0.06	0.14	-1.60	-1.52	-1.48
RMSE	0.23	0.23	0.26	1.13	0.96	0.89	2.05	1.93	1.88
m_{xy}	0.99	0.99	0.99	0.99	1.00	1.00	0.49	0.55	0.58
v_{xy}	0.99	0.99	0.98	0.71	0.74	0.77	0.69	0.73	0.75
R_{xy}	0.98	0.98	0.97	0.99	0.99	0.99	0.88	0.91	0.92

The mass balances at the glacier scale for the hydro year (April to March) 2012 and 2013 are show in Table 6 and illustrated in Figure 7. Table 6 provides the values of the annual (MB_A), summer (MB_S), and winter (MB_w) mass balances for the different study case, along with the results of glaciological measurements conducted by Kinnard and others (2018). In Figure 7, the mass balances of the ablation stakes installed by Kinnard and others (2018), are compared to the HRUs in which these stakes were placed. Also, the continuous lines show the 2^{nd}-order polynomial functions fitted. The calculated ELA corresponds to the elevation where the polynomial is equal to zero.

At the glacier scale, both calibrated models demonstrate good agreement with the glaciological mass balance of Kinnard and others (2018) as is shown in the Table 6. For the annual mass balance, with differences of less than -0.25 m.w.eq for the hydrological year 2012 and less than 0.43 m w.eq for the year 2013. These differences fall within the uncertainty range.

At the seasonal scale, the three models generally represent the winter mass balance well in 2012, although they underestimate accumulation values below 3100 m a.s.l. However, since the glacier area below this elevation accounts for only 12% of the total glacier, this discrepancy has minimal impact at the overall glacier level. Difficulties arise in replicating the steep gradient observed in the summer balance of 2012/2013, with overestimation of ablation in the higher elevations (3400-4000 m a.s.l.) and underestimation below 2800 m a.s.l. For the hydrological year 2013/2014, all three models experience a drop in performance, underestimating winter accumulation and summer ablation. In the glaciological mass balance, both years exhibit similar winter mass balances of 1.43 m w.eq (2012) and 1.48 m w.eq (2013). Capturing this similarity is challenging for the models due to the 27% lower winter precipitation in 2013 compared to 2012, as recorded by the la Rufina WS (Figure 1) and the meteorological gridded product used (3.1 section). Discrepancies in the gradients depicted in Figure 7 for the winter balance in 2013/2014 primarily occur above 3600 m a.s.l. This difference could be attributed to storms concentrated in the higher parts of the glacier or greater wind transport of snow from adjacent basins, phenomena intricately linked to the meteorological data used in the model.

For the summer mass balance of 2013/2014, all models slightly underestimate ablation by approximately 0.7 m.w.eq across the entire glacier. The underestimation of ablation in the summer of 2013/2014 can be primarily attributed to a higher number of sunny days compared to the summer of 2012/2013, resulting in increased incident radiation on the glacier (Kinnard and others, 2018), despite similar recorded air temperatures. Although the models incorporate incident radiation partly based on temperature, they were unable to fully capture the high ablation observed in 2013/2014. Despite these limitations, the models successfully reproduce the total mass balances of the glacier and closely follow the observed gradient.

Table 6: Comparison between seasonal and annual mass balance from different CHRM models and glaciological measurements from Kinnard et al. (2018).

	MB_w 12/13 (m.w.eq)	MB_S 12/13 (m.w.eq)	MB_A 12/13 (m.w.eq)	ELA 12/13 (m.w.eq)	MB_w 13/14 (m.w.eq)	MB_S 13/14 (m.w.eq)	MB_A 13/14 (m.w.eq)	ELA 13/14 (m.w.eq)
Glaciological mass balance	1.43±0.06	-1.75±0.38	-0.32±0.40	3478	1.48±0.15	-4.01±0.56	-2.53±0.57	4233
unc	1.46	-2.25	-0.79	3696	1.19	-3.73	-2.54	4066
difference (%)	2 (%)	-29 (%)	-147 (%)	218 (m)	-20 (%)	7 (%)	0	-167
	1.44	-2	-0.56	3689	1.20	-3.40	-2.20	4028
difference (%)	1	-14 (%)	-75 (%)	211 (m)	-19 (%)	15 (%)	13 (%)	-205
	1.48	-1.85	-0.37	3670	1.21	-3.31	-2.10	3998
difference (%)	3	-6 (%)	-16 (%)	192 (m)	-18 (%)	17 (%)	17(%)	-235

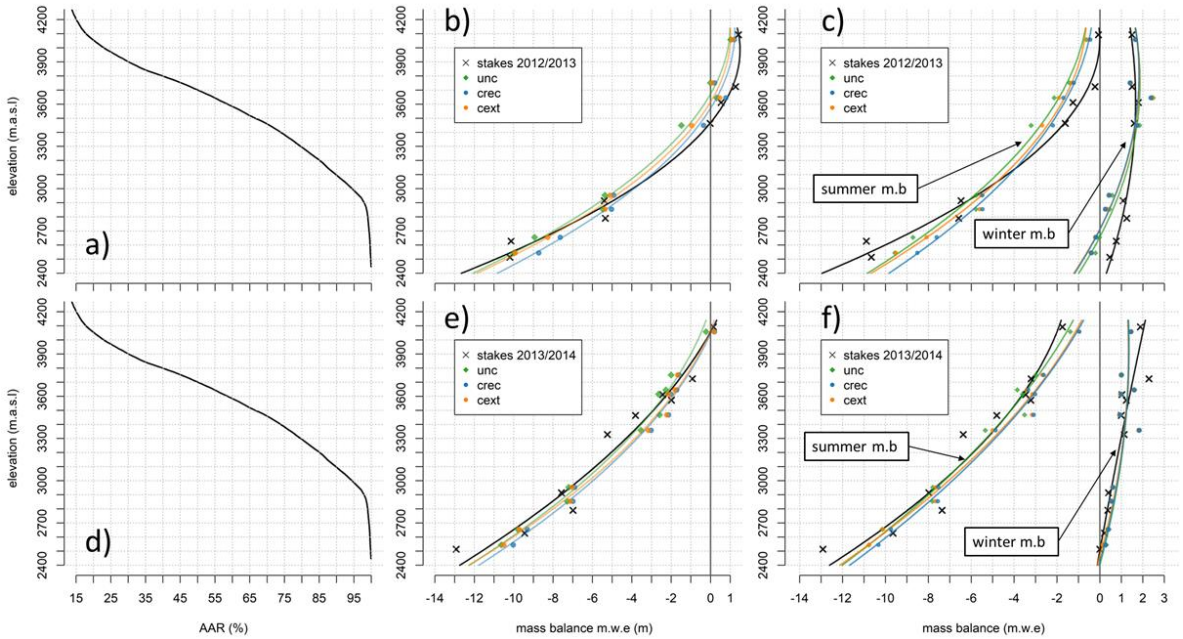

Figure 5: Measurements and modeled mass balances versus elevation. The black crosses represent the ablations stakes installed by Kinnard and others (2018). The color points represent the mean elevation and mass balance of the HRU where the ablation stakes were located. a) Annual mass balance for the hydro year 2012. b) seasonal mass balance for the hydro year 2012. c) Annual mass balance for the hydro year 2013. d) seasonal mass balance for the hydro year 2013.

4.3. Historical series

Figure 8 illustrates the cumulative mass balance for the Universidad glacier, derived from geodetic mass balances and modeled by different study cases. Panel (a) displays the cumulative mass balance from 1955 to 2020, while panel (b) focuses on the period from 2000 to 2020. Additionally, the cumulative mass balance of the Echaurren Norte Glacier, situated approximately 126 km north of the Universidad Glacier and serving as the reference glacier of the World Glacier Monitoring Service. The vertical dashed lines of the years 1971 and 2006 showed the change points find by the CUSUMs analysis conducted to the mass balance and showed in panel b of Figure 9.

As expected, given the different calibration objectives, the cext model exhibited better performance in the accumulated mass balance for the entire study period. The crec model overestimates the glacier losses by 34%, while the unc model overestimates by 38%. For the period between 2000-2020, characterized by significant glacier losses, the crec model performed better. The cext model showed an underestimation of glacier losses by 10%, while the unc model showed an overestimation of 26%.

Figure 9 presents the modeled mass balance for Universidad Glacier. In panel (a), the annual mass balance of the three cases is show, with red frames indicating NIÑA year (ONI < -0.5) light blue stripes indicating NIÑO years (ONI > 0.5). Panel (b) displays the CUSUM analysis of the modeled annual mass balances, whit the secondary axis showing the PDO anomaly. Blue frames point to the positive phases of PDO (PDO > 0) and red frames indicated the negative phases (PDO < 0). Table 7 shows the average mass balances and the standard deviation of the different models for the entire study period and the subperiod between the CP finding: 1955-1971, 1971-2006 and 2006-2019.

The three cases exhibit similar behavior, as shown in the annual mass balances in Figure 9. The main difference lies in the magnitudes of the mass balances, but they demonstrate almost equal interannual variability, as indicated by their close standard deviation in Table 7. Between the calibrated models cext and crec, there is an average bias of 0.26 m w.eq for the entire period, while the unc model and the crec model show a difference of 0.46 m w.eq. The difference in magnitude between the models does not affect the historical trends of the mass balance, as they identify the same statistically significant change points (p-value <0.04) in 1971 and 2006, as depicted by the dashed lines in Figures 8 and 9. There is also a slight difference between the models in the behavior of the different periods. While the the unc and crec models showed similar or equal mass balances for the period 1955-1971 and 2006-2019, while the cext calculate that the period 2006-2019 is the one that experienced the highest mass losses.

The difference between the models is explained almost entirely by the differences in the summer mass balance. While the percent bias between the models is equal to or less than 2% for the winter mass balance, for the summer mass balance, the difference between the unc and the cext models is -18%, while between the cext and the crec is -8%.

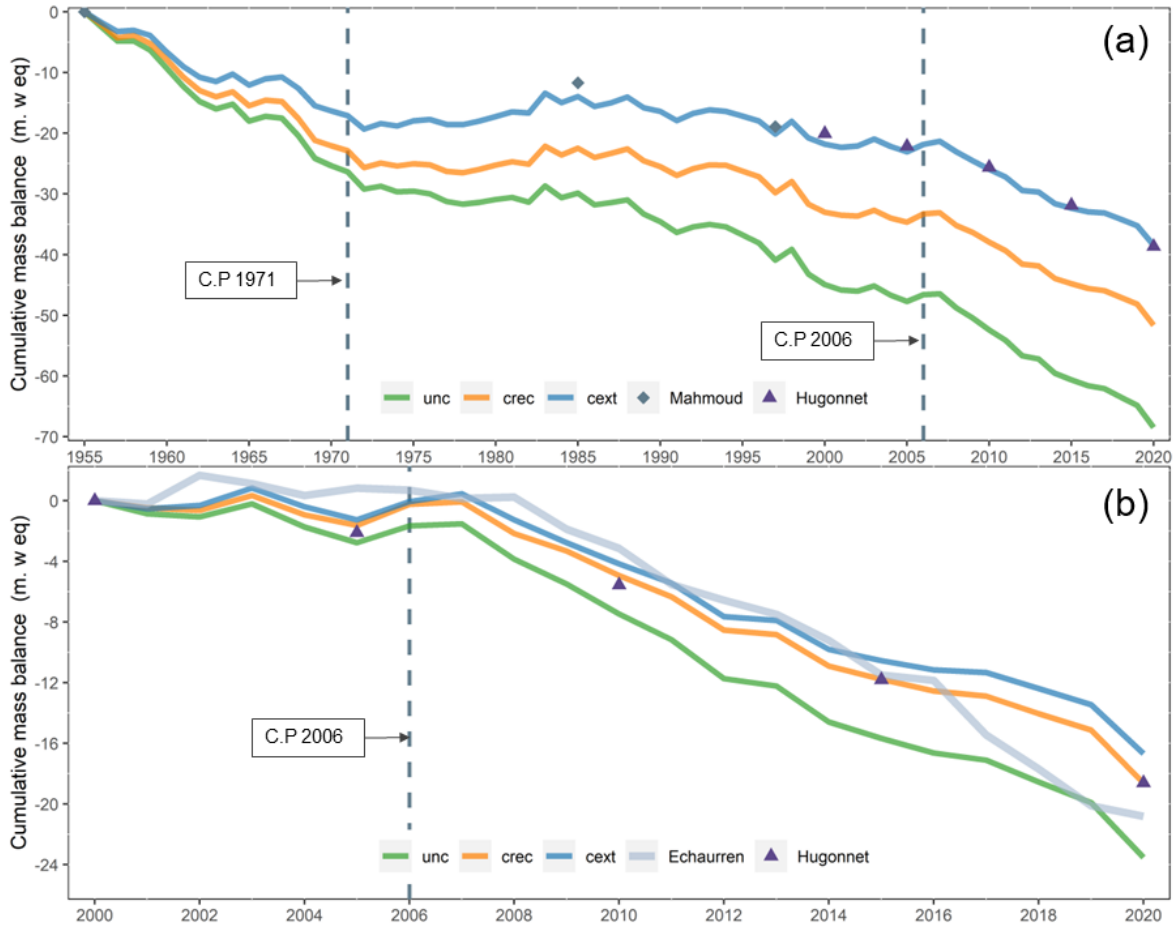

Figure 8: Upper panel: Cumulative mass balance series of the different CRHM models, the gray squares and purple triangles correspond to the cumulative mass balance calculated from the BMGs of Mahmoud and others (2022) (gray squares) and Hugonnet and others (2021) (purple triangles). Lower panel: cumulative mass balance of the different CRHM models since 2000, the gray line corresponds to the cumulative mass balance of the Echurren Norte glacier.

In terms of glacier evolution, the CUMSUM analysis of mass balance identified two statically significant change points. The first change point in 1971 marked the end of a period characterized by sustained glacier mass loss from 1955 to 1971, where only four years experienced a positive or near-equilibrium mass balance (Figure 9a). This period is evident in the continues decay in the CUMSUM analysis (Figure 9b) and the cumulative mass balance (Figure 8a). The models showed high ablation rates during this period, with -2.53 m.w.eq for the cext model.

Between 1971 and 2006, there was a period near-equilibrium period in the mass balance for the Universidad glacier, with the cext model showing an average mass balance of -0.07 m.w.eq. In the early years of this period (1972-1982), the models exhibited a positive mass balance, with almost all the years having positive or neutral mass balances. This is clearly seen in the continuous upward slope in the CUMSUM analysis, and the models calculated average mass balances of 0.54 (cext), 0.35 (crec), and 0.05 (unc) m.w.eq y^{-1}. This positive period is followed by a slightly negative period of cumulative mass balance between 1982-

2006, with all models calculating average negative mass balances (cext -0.22; crec -0.34; unc -0.64 m.w.eq y^{-1}). Despite the different behaviors of these two subperiod, with the first one characterized by small variability and continuous years of positive mass balance, and the second one with high interannual variability and average negative mass balance, were not identified as statistically significant change points.

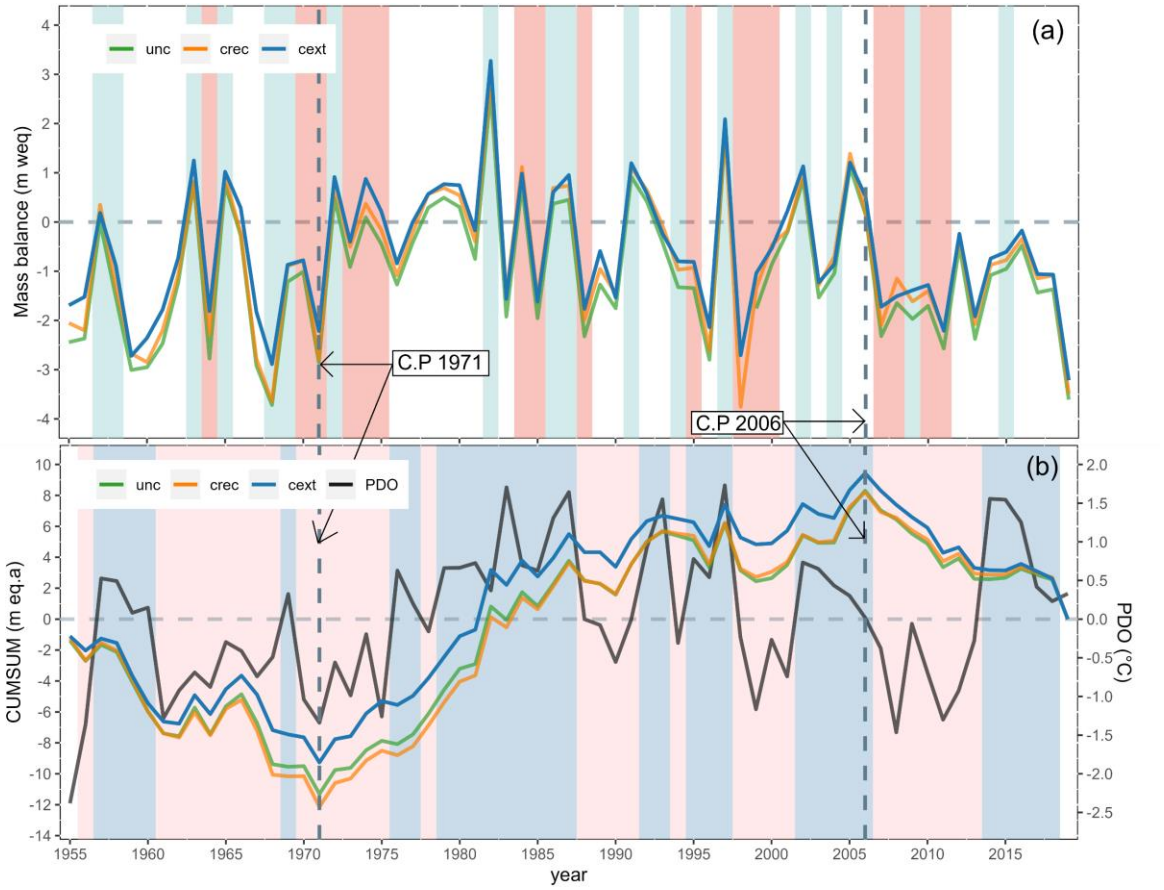

Figure 9: a) Series of annual mass-balance of the different CRHM, the NIÑA years are the red frames, while the blue light frames correspond to NIÑO years. B) CUMSUM analysis for annual mass-balance and the PDO index. The grey dotted line corresponds to the statistically significant CP found through CUSUM and verified with Pettitt's test (p-values < 0.04).

The second change point in 2006 marks a period of sustained mass loss, characterized by the lowest mass balance average, primarily driven by the lowest winter mass balances calculated. Additionally, this period exhibits the lowest interannual variability. Since 2007, no year has shown a positive balance, with only 2012 and 2016 being close to equilibrium. This turning point is clear in the cumulative mass balance since 2000 (Figure 8b), where a sharp decline is observed since 2007, after a period of near equilibrium.

The annual mass balances exhibit a moderate temporal correlation with the ENSO phenomenon, with an r-spearman of 0.41. It is also noteworthy that, for the 18 years in which all the models calculated positive mass balances, nine correspond to NIÑO years, two NIÑA years and seven to neutral years. Additionally, all the strong NIÑO years ($1.5 \leq ONI < 2$) are hydro-years with positive mass balance: 1957, 1965, 1972, 1987, 1991 with 0.18, 1.02, 0.91,

1.12, and 1.19 m.w.eq, respectively, for the cext model. Since 1950, there have been only three NIÑO very strong events: 1982, 1997, and 2015. Of these events, 1982 and 1997 correspond to the highest modeled mass balances of 3.27 and 2.09 m w.eq, respectively for the cext model.

The CUSUM analysis and, consequently, the identified change points show a relationship with the predominant phases of PDO. Although the correlation between the PDO and the CUSUM analysis for the entire period is weak, with an r-spearman of 0.32, this relationship becomes more apparent before the second change point, with an r-spearman of 0.52 between the years 1955-2006, corresponding to a moderate correlation. The first period identified from 1955 to 1971 is mainly dominated by negative years of PDO anomaly, with a negative PDO phase from 1960 to 1974. Although the point of change in 1971 does not coincide directly with the PDO phase change, a clear positive trend is observed (p-values MK test < 0.01) that clearly coincides with the CUSUM analysis, both starting in 1971 and ending in 1986. The second period delimitated between the change points in 1971 and 2006 is mainly characterized by a positive phase of the PDO which begins in 1976 and finished near 2006 (Boisier and others, 2016). From the second point of change, the relationship between the ENSO and PDO phenomena and the interannual variability of the mass balances is lost, as can be seen in the decay of the spearman correlation. For the ENSO-annual mass balance correlation if we consider the period 1955-2019 the value is 0.41, while for the years 1955-2006 the value is 0.47. For the PDO-CUSUM correlation the difference decay is more clearly, from 0.52 to 0.32. The positive phase of the PDO since 2014 does not have influence in the cumulative mass balance, showed a continuation of the negative trend initiated in 2008 (Figure 9 b).

Table 7: Mean m.w.eq and standard deviation (Stdv) m.w.eq of the annual and seasonal mass balances for the whole period and between years identified as change points for the: unc, crec and cext models. The percentage bias (Pbias) is in reference to the cext model.

		Annual mass balance			**Winter mass balance**			**Summer mass balance**		
Period	**Metric**	**unc**	**crec**	**cext**	**unc**	**crec**	**cext**	**unc**	**crec**	**cext**
1955/ 2020	Mean	-1.05	-0.79	-0.59	1.89	1.89	1.91	-2.94	-2.69	-2.50
	Stdv	1.40	1.39	1.29	0.97	0.98	0.97	0.68	0.64	0.60
	MAE	0.46	0.26	-	0.02	0.02	-	0.44	0.25	-
	Pbias	-78	-34	-	1	1	-	-18	-8	-
1955/ 1971	Mean	-1.65	-1.43	-1.07	1.44	1.44	1.46	-3.09	-2.87	-2.53
	Stdv	1.36	1.34	1.21	0.75	0.76	0.76	0.80	0.76	0.71
	MAE	0.58	0.39	-	0.02	0.02	-	0.56	0.37	-
	Pbias	-58	-34	-	1	1	-	-22	-14	-
1971/ 2006	Mean	-0.51	-0.22	-0.07	2.33	2.33	2.35	-2.84	-2.56	-2.42
	Stdv	1.36	1.32	1.25	1.00	1.00	0.99	0.59	0.54	0.49
	MAE	0.44	0.22	-	0.02	0.02	-	0.42	0.21	-
	Pbias	-592	-203	-	1	0.06	-	-17	-6	-
2006/ 2019	Mean	-1.69	-1.43	-1.32	1.30	1.31	1.33	-2.94	-2.69	-2.50
	Stdv	0.85	0.84	0.80	0.50	0.50	0.50	0.58	0.63	0.50
	MAE	0.37	0.17	-	0.03	0.02	-	0.35	0.15	-
	Pbias	-28	-8	-	2	1	-	-13	-4	-

4.4. Equilibrium-line altitudinal and glacier albedo

To evaluate the performance of the different models in simulating total glacier albedo, the albedo values calculated by Shaw and others (2020) were compared with the weighted albedo values of each URH. Table 7 shows the performance of the models between the years 1990 to 2019, the years where Shaw and others (2020) images are available.

Among the models, the cext model demonstrates the best performance, with the lowest RMSE of 4% and the highest temporal correlation of 0.71. All three models exhibit a negative bias, particularly struggling to replicate the highest albedo values observed during the years 1995-2001, as shown in the temporal albedo presented in the supplementary material. Nonetheless, as is observed in Table 9, the models that undergo the calibration process (cext and crec), reduce the bias by more than half compared to the uncalibrated model.

Table 8: Metrics of the albedo performance against the estimated albedo through Landsat imagery by Shaw and others (2020)

Metric	unc	crec	cext
RMSE (%)	6	5	4
R2 (-)	0.36	0.45	0.50
Pbias (%)	-9.8	-3.2	-0.8
Spearman correlation (-)	0.52	0.67	0.71

Figure 10 illustrates the evolution of the ELA for the different study cases, accompanied by the CUMSUM analysis to identify change points. The cext model consistently exhibits the lowest ELA, aligning with its higher mass balances. On average, the differences between the cext and the unc models are 31 m, and between the unc and crec model is 20 m.

Considering that the ELA falls between 3630 and 3960 m a.s.l in 50% of the years, the percentage difference in terms of area change in the AAR is approximately 3% of the glacier for every 30 meters of elevation (Figure 7a). In other words, there is approximately. 3% less accumulation area in the unc model compared to the cext, and 2% less in the crec compared to the cext model. As for the mass balances and glacier discharge, the three models exhibit the same change and points and trends.

In the CUMSUM analysis, we identified the same change points as in the mass balance: 1971 and 2006. The period between 1955 and 1971 is characterized by high interannual variability and no clear trend. The second period between 1971 to 2006 exhibits a lower average ELA, while the period from 2006 to 2019 shows a higher average ELA and lower deviation. Since 1971, we found a statistically significant trend of 35 m per decade.

In Table 6, the comparison between the models ELA and the glaciological balance for the years 2012 and 2013 shows an overestimation of the ELA by around 200 meters for the year with the highest mass balance, and an underestimation for the year with the lowest mass

balance. Considering that the spatial discretization of the HRU is approximately 100 m of elevation, the discrepancy in the location of the ELA is within two or three HRU.

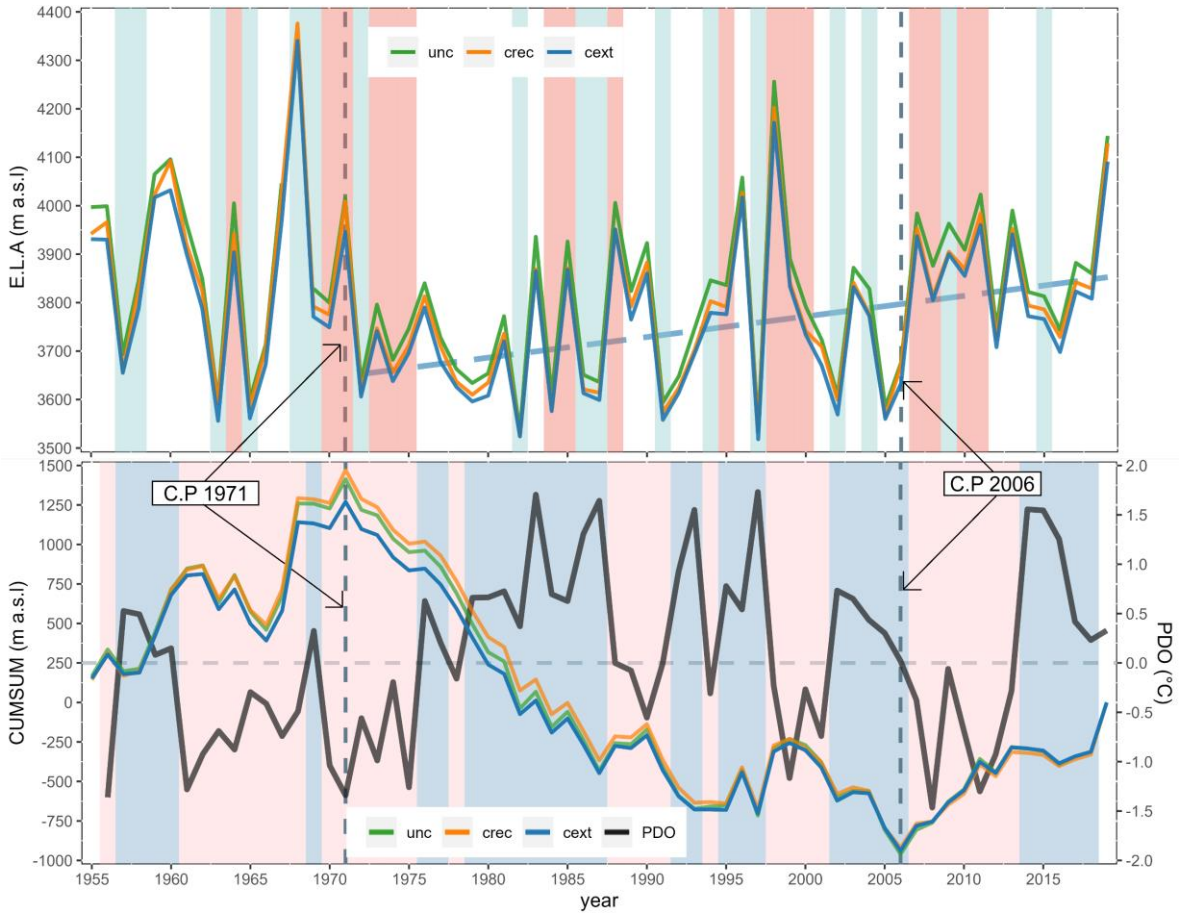

Figure 10: a) Series of annual mass-balance of the different CRHM, the NIÑA years are the red frames, while the blue light frames correspond to NIÑO years. B) CUSUM analysis for annual mass-balance and the PDO index. The grey dotted line corresponds to the statistically significant CP found through CUSUM and verified with Pettitt's test (p-values < 0.04).

4.5. Glacier Runoff

Figure 11 (a) illustrates the annual average glacier discharge from the Universidad glacier for the three cases. Glacier discharge is computed as the sum of firn and ice melt by the model, excluding runoff from the accumulated and depleted snowpack within the same year. Figure 10 (b) presents the CUMSUM analysis of the annual average glacier discharge alongside the PDO anomalies. Figure 10 (c) shows the contribution of the Universidad glacier to the Tinguiririca Bajo Los Briones Basin. This contribution is calculated as the glacier discharge simulated by the model for the summer months (Jan-Feb-Mar), divided by the observed streamflow at the fluviometric station located at the basin's exit.

The difference between the models exhibits a similar pattern as in the mass balance, primarily showing a bias but maintaining a comparable interannual variability. This is evident in the similar deviation of the modeled series. The percent bias between the cext model, consider as reference, and the unc and crec models remains consistent throughout the study period.

The unc model, characterized by more negative mass balances, yields a higher water contribution, overestimating glacier runoff by 14% compared to the cext model. In contrast, the crec model shows a slightly lower overestimation of approximately 7%. These differences undergo a minor percentage reduction when analyzing the summer runoff, with a -12% difference between the unc and cext models and -5% between the crec and cext models.

Due to this almost identical behavior in the year-to-year variations of the models, the analysis of change points and trends yields consistents results. In the CUSUM analysis, two statistically significant change points were identified: 1971 and 1993.

The first period between 1955 to 1971 is characterized by a highly average discharge and highly interannual variability, been the maximum in both statistics in the entire period. The change point is the same that encountered for the mass balance and emerges clearly in the CUSUM analysis due to the high number of years with an average discharge above the historical average for 1955-2019.

Between 1971 and 1993, there is a period with a relative low glacier discharge due to the neutral mass balance between 1972 and 1982. In the second half of this period, there is considerable great interannual variability in the annual discharge. The second change point in 1993 is attributed to the occurrence of four la NIÑA events between 1995 and 2000, leading to a decrease in precipitation and an increase in temperature compared to the preceding years since 1971. This results in a significant increase in the magnitude of the ice and firn melt between 1995 and 2000, clear in the change in slope in the CUSUM during those years. In 2006, there is also a change in slope, coinciding with the change point for the mass balance, but this change is not statistically significant according to the Pettit test.

From the first change point in 1973, there is an increasing trend in glacier discharge of 0.18 m^3/s per decade for all the models. This corresponds to a 10% increase in the simulated runoff from the cext model. All the models identified the same trend with the same statistically significant of p-value of the Mann-Kendall test, which is < 0.02.

Regarding the relationship between ENSO and glacier discharge, there is an inverse moderate correlation with an r-spearman of -0.46. For the interannual variability, the relationship between the CUSUM and the PDO is -0.35, indicating a weak correlation. Similar to the mass balance, the relationship between ENSO and PDO is stronger than before the 2010s decade. Consider the period until the second change point (1955-1993), the correlation between the PDO and the CUSUM is -0.6, indicating a considerable increase. Even if we consider the period between 1955-2006, the second change point for the mass balance, the correlation is of -0.51. In the case of ENSO, for the period before the second change point, the correlation is maintained, but when considering the period between 1955-2006, the correlation increases to -0.55.

Table 9: Mean annual mean glacier runoff (Mean) and its standard deviation (Stdv) (m3/s) for the whole period (1955-2019) and between the years identified as change points for the uncalibrated and calibrated models. The percentage bias (Pbias %) refers to the model calibrated with the extended period. Glacier discharge is calculated as firn and ice melt.

		Annual discharge			**Summer discharge**		
Period	**Metric**	**unc**	**crec**	**cext**	**unc**	**crec**	**cext**
1955/ 2020	Mean	1.59	1.46	1.48	4.88	4.49	4.49
	Stdv	0.62	0.57	0.47	1.65	1.55	1.31
	MAE	0.19	0.08	-	0.63	0.24	-
	Pbias	-14	-4	-	-15	-5	-
1955/ 1971	Mean	1.89	1.77	1.66	5.47	5.10	4.74
	Stdv	0.69	0.63	0.55	1.89	1.80	1.76
	MAE	0.23	0.12		0.73	0.37	-
	Pbias	-14	-6	-	-16	-8	-
1971/ 1993	Mean	1.18	1.08	1.04	3.95	3.61	3.47
	Stdv	0.36	0.30	0.27	1.03	0.87	0.87
	MAE	0.14	0.04	-	0.50	0.14	
	Pbias	-14	-4	-	-14	-4	-
1993/ 2019	Mean	1.71	1.56	1.50	5.20	4.75	4.52
	Stdv	0.54	0.50	0.48	1.55	1.45	1.42
	MAE	0.21	0.08	-	0.68	0.23	-
	Pbias	-14	-4	-	-15	-5	-

The Universidad glacier, which covers only 2% of the Tinguiririca Bajo Los Briones basin (1438.3 km^2, Figure 1), has made a significant contribution to the overall runoff of the watershed, particularly in the summer seasons. Considering the runoff observed by the station at the basin outlet (Figure 2) and that simulated by the model, for the years with sufficient observations (over 80% of the days with data), the cext model, which estimates the lowest ice melt, shows that the annual contribution ranged from 1% in 2002 to 19% in 2019, with an average during all study period of 5%.

During the summer months (Dic-Mar), which are when most of the glacial runoff occurs, the relative contribution of the Universidad Glacier becomes especially relevant. The summer contribution has ranged from 3% in the years 1963, 1997, and 2002 to a unique maximum of 38% for the cext model.

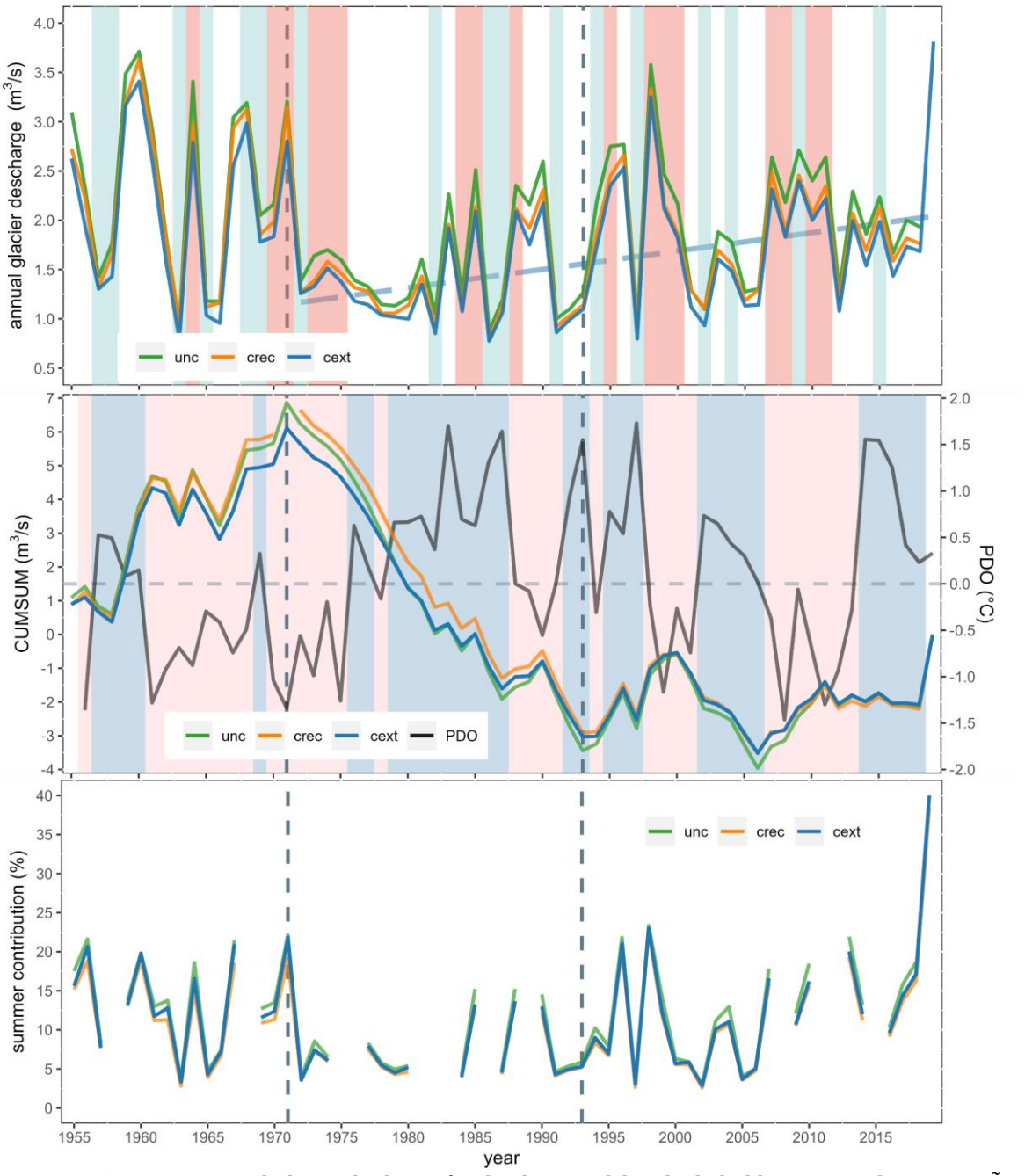

Figure 11: a) Average annual glacier discharge for the three models. The light blue stripe indicates a NIÑO year, while the red stipe indicates a NIÑA year. The dashed blue line from 1971 to 2019 indicates a statistically significant increasing trend. b) CUSUM analysis for the annual glacier discharge with the PDO anomaly. The blue stripes indicate positive phases of PDO, while red stripes indicate negative PDO phases. c) Relative contribution of the Universidad glacier ice melt to the entire Tinguiririca Bajo Los Briones basin (Figure 1c) for the summer months (Jan-Feb-Mar).

5. Discussion

5.1. Parameter sensitivity and Calibration

It is reasonable to expect that the most sensitive parameters are related to albedo, as shortwave radiation plays a crucial role in driving glacier ablations processes (Munro, 1982). The successful calibration of the cext model, emphasizing a reduced number of highly-sensitive parameters within a physically reasonably range, demonstrates that a physical-based energy-balance model can effectively represent the mass balance in a long-term simulation. This suggests the potential application of such modeling approaches for extended periods of time.

Moreover, the annual variability of the mass balance exhibits striking similarities between the calibrated models (cext and crec) and the model without calibration, enabling the identification of trends and periods across the models. This suggests that a physically-based model without calibration, but with a judicious selection of parameters, holds significant utility for studying the annual behavior of glaciers variables such as mass balances or runoff.

The biggest differences in the results of the models emerges in the cumulative mass balances, due that the between the models there are differences in the ablations rates. Although the differences vary from period to period, the unc model always presents the highest ablations, while the cext model is that experiences the lowest ablation. This constant difference causes that the cumulative mass balance differs in a considerable way at the end of the simulated period. This can have a significant impact when calculating projections or reconstructions of glacier volume.

As example, based on Radio-Echo Sounding data, the total volume of glacier was estimated to be 1.63 km^3 w.eq in 2012 (DGA, 2012). Assuming the same area as in 2010 and using the calculated GMB, we estimate a volume of 2.49 km^3 w.eq in 1955. Calculating the volume loss with the different models, starting from the 2.49 km^3 w.eq in 1955, the unc model indicates a volume loss of 72%, the crec model a loss of 54%, while the cext model a loss of 44%.

5.2. Universidad glacier mass balance evolution

The periods and the evolution of the Universidad Glacier found by our model are consistent with the results of different glacier studies in the central Andes. Masiokas and others (2016) modeled the Echaurren Norte glacier, the same glacier shows as a reference in Figure 8, located up to 126 km north of the Universidad glacier. Masiokas and others (2016) identified a period of sustained loss from the 1940s to the early 1970s. On the other hand, Ayala and others (2020), in their modeling of the Maipo Basin (33º to 34º) found a nearly neutral period between 1955 and 1968, followed by a more negative mass balance between 1968 and 1975. Our results aligned well with of the Masiokas and other (2016), depicted that their methodology is based in simply correlation between register temperatures and mass balances, pointing that the Universidad glacier and the Echaurren Norte glacier can have similar responses. This fact is also represented in the correlation finding between ENSO and the mass balance of the Echaurren Norte glacier (Farías-Barahona and others, 2019). Our

difference between our study and Ayala and others (2020) for the period 1955 to 1968 could be attributed to climatic differences in the study areas or the lower elevation of Universidad glacier compared to the average elevation of the glaciers modeled by Ayala and others (2020) (3800 m a.s.l) for their southernmost sub-basin, which is closet to Universidad glacier.

Wilson and others (2016) investigated fluctuations in surface ice velocity of the Universidad glacier between 1967 and 2015 through different satellites images. They recorded a retreat of 177 m in Universidad glacier between 1969 to 1985, along with an increase in glacier surface velocity in 1985 compared to 1969. The significant mass loss modeled between 1955 to 1971 explains the observed retreat, while the period of slight mass gain between 1971 and 1982 accounts for the increased velocity of the glacier.

Between the period of 1971 to 2006, there are two brief periods of equilibrium: 1991-1993 and 2001-2006 observed as an upward slope in the CUMSUM analysis (Figure 10). These periods are correlated with slight increase in ice surface velocity and glacier fronts advances (Wilson and others, 2016). Wilson and others (2016) postulate that the observed increases in ice velocity could be due to periods of positive mass balance experienced by the Universidad glacier, due to the relationship between mass balance and ice velocity. However, the presence of a surge registered by Lliboutry (1958) in 1943 hinders this hypothesis, as the velocity increases could be attributed to surge cycles specific to the glacier.

Our results are consistent with the observations of Wilson and others (2016), revealing the presence of positive mass balance cycles in the Universidad glacier. This supports the hypothesis that the ice speed is influenced by this behavior. The agreement between our findings and those of Wilson and others (2016) underscores the underexplored potential of estimating mass balance through the relation between changes in ice surface velocity obtained from optical-historical imagery. This approach can be used to corroborate and complement these results with mass balances simulations.

Because the developed model does not adjust the glacier geometry due to mass loss or gain, it could be categorized as a reference-surface balance (Elsberg and others, 2001). This type of mass balance may underestimate mass loss when using the glacier geometry at the end of the simulation period, as is the case of our Universidad model, or overestimate mass loss when using the initial glacier geometry (Huss and others, 2012). Although calibrated models may underestimate mass loss, Huss and others (2012) observed that the interannual variability of mass balances and trends did not differ significantly when comparing a fixed geometry model versus a geometry-adjusted model. They noted that the largest long-term differences depended strongly on the retreat of the glacier, with the glaciers whose tongues had steeper slopes showing the largest discrepancies.

In the case of the Universidad glacier, we observed that the glacier terminus has a gentle slope (Figure 2). This is also supported by the fact that the Universidad glacier has experienced a moderate retreat versus others glacier in the semi-arid Andes, with only 6% of their area reduced between 1945 to 2011. For instance, Juncal Sur, Olivares Alfa, Olivares Beta, and Olivares Gamma glaciers have lost 34%,32,37%, and 20%, respectively (DGA, 2011).

5.3. Runoff and ELA

Our findings reveal notable interannual variability in glacier discharge and its contribution to the Tinguiririca Bajo Los Briones runoff, particularly during the summer months, with values ranging from 3% to 38%. In the summer of 2009/2010, Bravo and others (2017) estimated a contribution of 10-13% from the Universidad glacier, considering both ice melt and snow melt. For the same period, the cext model, which calculates the lower contribution, estimates 12%, considering the ice, firn, and snow melt. Since the area used by Bravo and others (2017) is 29 km^2, corresponding to the limits of the glacier in 2000, which is 11% larger than the area recorded in 2020 used in this study, our estimates of ablation are slightly larger than those estimated by Bravo and others (2017). These differences can be attributed to the variations in the modeling approach used. While Bravo and others (2017) used a distributed degree-hour model, calibrated at a punctual scale, and forced with local meteorology from an AWS, we used an Energy-balance model forced with reanalysis products. Additionally, Bravo and others (2017) did not estimate the effects of debris cover on the glacier tongue. While Bravo and others (2017) suggest that not considering the effects if debris could lead to an overestimation in the glacier tongue, recent works suggest that debris can accelerate the process of ablation (Rounce and others, 2021).

Respect to other regionals studies, Ayala and others (2020) for the Maipo Basin also find a strong annual variability in the glacier contribution, calculated that the ice melt can vary from less than 10% to more than 90% as in the year 1968/1969. For the year 1968/1969 we calculate the fourth highest glacier discharge, but due the lack of streamflow recording for that years it is not possible to calculate the summer contribution. In terms of magnitude, for the period 1955 to 2015 Ayala and others (2020) calculated a runoff from the ice melt of 596 mm yr^{-1} for the Maipo glaciers. This is considerably lower than our calculus of 1635 mm yr^{-1} for the same period. This difference can be attributed to the elevation range of the glaciers study by Ayala and others and present in the Maipo Basin are in a mean elevation considerable higher than the elevation range of the Universidad Glacier, with only a few glaciers covers altitudes lowers than 3000 m a.s.l. Additionally, the presence of debris-covered glaciers with lower ablation rates can decrease the average ice melt contribution.

The increasing trend in glacier discharge observed between 1971 and 2019 aligns with the projections made by Escanilla-Minchel and others (2020). Using a degree-day model, they projected changes in glacier runoff for the period 2020-2100, with a reference period of 2008-2014. Their findings indicate that glaciers will experience an increase in runoff for the RCP 4.5 and RCP 8.5 scenarios until around 2040, followed by gradual decline in glacier runoff. This suggests that the peak water of this glacier has not been reached, which is consistent with our estimates of an increase in trend.

Ayala and others (2020) did not identify a trend in the glacier runoff, suggesting that the large interannual and inter-decadal variation in precipitation could obscure pointing runoff trends of glaciers. Our study, along with the findings of Escanilla-Minchel and others (2020), suggest the possibility of a peak water scenario for the Universidad Glacier. The discrepancy with Ayala and others (2020) may be attributed to climatic differences between the basins or the regional behavior of different glaciers potentially masking trends in individual glaciers.

Within less than 14 km from the Universidad glacier, there are four other glaciers: Cipreses Norte, Cipreses, Cortaderal, and Palomo B, covering a combined area of 58 km^2. The presence of a potential trend in the Universidad glacier raises the possibility that these nearby glaciers might also experience an increase in runoff. This hypothesis should be explored in future studies.

In the evolution of the ELA, our results indicate an increase of 35 m per decade in the glacier since 1971. This rise in the ELA impacts the glacier's mass balance, resulting in an approximately 8% reduction in the accumulation area for every 100 m of elevation (Figure 7a).

A positive trend in ELA elevation is also observed for the Maipo glaciers by Ayala and others (2020), with an increase of 39 m per decade between 1955 and 2015. Barria and others (2019), using a relationship between the 0-degree isotherm altitude (ZIA) and precipitation, derived an estimate of the ELA at regional scale (between 33-34S). They found a statistically significant trend in the ELA elevation of 64 ± 8 m per decade for the period 1978 to 2018. Additionally, Barria and others (2019), through a CUSUM analysis, identified an abrupt change in the ZIA in the year 1976, close to our change point in 1971. The variations in our finding could be attributed to methodological differences, and Barria and others (2019) focusing on regional estimates. Despite differences in the magnitude of the trend and change points with Barria and others (2019) and Ayala and others (2020), our results are consistent revealing the presence of an increasing trend in ELA since at least the mid-1970s.

6. Conclusions

To explore the potential advantages of integrating geodetic mass balances into calibration process of physically-based glaciological model, three case studies were conducted: an uncalibrated model (unc), a calibrated model utilizing GMB from a recent period (2000-2020) characterized by more pronounced ablation (crec), and a calibrated model employing a GMB from the entire analysis period (1955-2020), encompassing some periods of neutral or even slightly positive mass balances.

The three cases analyzed exhibit a moderate correlation between the Pacific Decadal Oscillation and long-term mass balances. Positive phases of the PDO coincide with period of slightly positive or neutral mass balances, while negative phases align with pronounced periods of mass loss. Additionally, the ENSO phenomenon demonstrates a moderate relationship with annual mass balances, where the years of strong-very strong NIÑO years events correspond to positive ENSO phases and larger accumulation. However, since the initiation of the megadrought in 2010, this relationship has been interrupted, leading to a loss of correlation.

Regarding the evolution of the Universidad glacier this has shown three distinct periods: a period of significant mass loss between 1955 and 1976, followed by a period of almost equilibrium between 1976 and 2006, and finally, another period of substantial loss between 2006 and 2020.

It is crucial to emphasize the significance of the PDO in influencing long-term mass balances. When conducting glacial simulations covering extended periods spanning several decades, it becomes essential to account for the effects of the PDO. This underscores the importance of considering replicability of climate patterns, particularly the PDO and the ENSO phenomenon, when making projections of mass balance in glacier studies.

At the site scale, no model shows a clear superiority when compared to in-situ records of albedo and snowpack height. Although all three models accurately represent the measurements at the automatic meteorological stations located in the ablation zone between 2012 and 2014, they face greater difficulties in reproducing the variables recorded by the stations located in the accumulation zone. Regarding the glacier mass balance for the years 2012-2013 and 2013/2014, the model calibrated with the extended period demonstrates slightly better performance as it exhibits the lowest average error for the two years with glaciological mass balance data.

The calibration process using Geodetic Mass Balances allows for the adjustment of a limited number of physically plausible parameters, leading to an improvement in model performance. In the cext and crec models, the overestimation of ablation was mitigated, and the total albedo of the glacier at the daily scale exhibited enhanced performance, resulting in an improved representation of hydro-glaciological processes. While the annual scale differences between the models are small, their cumulative effects become significant over the long term. This is particularly crucial for glacier volume projections in climate change studies.

The runoff has shown a growing trend of 8% per decade since 1971, mainly driven by the increase in the Equilibrium Line Altitude (ELA) and the expansion of the ablation area. This trend is consistent with the findings of the study conducted by Escanilla-Minchel and others. (2020), which identified a peak in water flow around 2040, reinforcing the hypothesis that the glacier has not yet reached its "peak water." Considering the presence of other significant glaciers within an 18 km radius of Glaciar Universidad, such as Cortaderal (14.7 km2), Palomo (14.5 km2), and Cipreses (22.2 km2), there is a possibility that a substantial part of the semi-arid Andean glaciers' area has not yet reached its maximum water flow. To determine if the maximum water flow has indeed not been reached in the region, further glacio-hydrological modeling studies covering a historical period and projections are needed.

Improving our understanding of Glaciar Universidad and other glaciers in the region regarding their contributions to the total flow of the basin is crucial. We have calculated that Glaciar Universidad contributes on average 5% to the Tinguiririca basin flow at Bajo los Briones, and in 2019, it represented 39% of the summer flow. This contribution is significant, considering that the Tinguiririca River provides drinking water to 100,000 people and supports vital economic activities such as hydroelectric power generation and highly productive valleys like the Colchagua Valley, renowned for its wine production.

As a future research direction, we suggest further investigation into the effects of calibration with geodetic mass balances using different data sources for the same temporal periods. This

approach will help address the consequences of the strengths and weaknesses of each method employed and enhance the accuracy and reliability of the modeling results.

Acknowledgments

AM was partially supported by the project FONDECYT 1201429 and the grant ANID-MAGISTER NACIONAL 2021 folio 22211060.

III. CONCLUSIONES

Para explorar las posibles ventajas de integrar balances de masa geodésicos en el proceso de calibración de modelos glaciológicos basados en la física, se llevaron a cabo tres estudios de caso: un modelo no calibrado (unc), un modelo calibrado utilizando balances de masa geodésicos de un periodo reciente (2000-2020) caracterizado por una ablación más pronunciada (crec), y un modelo calibrado utilizando balances de masa geodésicos de todo el periodo de análisis (1955-2020), abarcando algunos periodos de balances de masa neutra o incluso ligeramente positivos.

La evolución del glaciar Universidad esté ha mostrado tres periodos distintos: un periodo de pérdida significativa de masa entre 1955 y 1976, seguido por un periodo de casi equilibrio entre 1976 y 2006, y finalmente, otro periodo de pérdida sustancial entre 2006 y 2020.

Los tres casos analizados muestran una correlación moderada entre la Oscilación Decadal del Pacífico y los balances de masa a largo plazo, con valores de la correlación de spearman de 0.52 entre los años 1955-2006. Las fases positivas de la PDO coinciden con periodos de balances de masa ligeramente positivos o neutros, mientras que las fases negativas se alinean con periodos pronunciados de pérdida de masa. Además, el fenómeno ENSO muestra una relación moderada con los balances de masa anuales, donde los años de eventos fuertes-muy fuertes de NIÑO corresponden a fases positivas del ENSO y una mayor acumulación. Sin embargo, desde el inicio de la megasequía en 2010, esta relación se ha interrumpido, llevando a una pérdida de correlación.

Es crucial enfatizar la importancia de la PDO en la influencia de los balances de masa a largo plazo. Esto destaca la importancia de considerar la replicabilidad de los patrones climáticos, especialmente la PDO y el fenómeno ENSO, al hacer proyecciones de balances de masa en estudios glaciares.

A escala del sitio, ningún modelo muestra una superioridad clara en comparación con los registros in situ de albedo y altura de la capa de nieve. Aunque los tres modelos representan con precisión las mediciones en las estaciones meteorológicas automáticas ubicadas en la zona de ablación entre 2012 y 2014, enfrentan mayores dificultades para reproducir las variables registradas por las estaciones ubicadas en la zona de acumulación. En cuanto al balance de masa glaciar para los años 2012-2013 y 2013/2014, el modelo calibrado con el periodo extendido muestra un rendimiento ligeramente superior, ya que presenta el error promedio más bajo para los dos años con datos de balance de masa glaciológica.

El proceso de calibración utilizando Balances de Masa Geodésicos permite ajustar un número limitado de parámetros físicamente plausibles, lo que mejora el rendimiento del modelo. En los modelos cext y crec, se representó mejor la ablación, y el albedo total del glaciar a escala diaria mostró un rendimiento mejorado, lo que resulta en una representación mejorada de los procesos hidro-glaciológicos. Aunque las diferencias a escala anual entre los modelos son pequeñas, sus efectos acumulativos son significativos a largo plazo. Esto es especialmente crucial para las proyecciones de volumen glaciar en estudios de cambio climático.

El caudal ha mostrado una tendencia creciente del 8% por década desde 1971, impulsada principalmente por el aumento de la Altitud de la Línea de Equilibrio (ELA) y la expansión de la zona de ablación. Esta tendencia es consistente con los hallazgos del estudio realizado por Escanilla-Minchel y otros (2020), que identificaron un máximo en el flujo de agua alrededor de 2040, reforzando la hipótesis de que el glaciar aún no ha alcanzado el máximo rendimiento hídrico. Considerando la presencia de otros glaciares significativos dentro de un radio de 18 km del Glaciar Universidad, como Cortaderal (14.7 km2), Palomo (14.5 km2) y Cipreses (22.2 km2), existe la posibilidad de que una parte sustancial del área de los glaciares semiáridos andinos aún no haya alcanzado su máximo flujo de agua.

Mejorar nuestra comprensión del Glaciar Universidad y otros glaciares en la región con respecto a sus contribuciones al flujo total de la cuenca es crucial. Hemos calculado que el Glaciar Universidad contribuye en promedio con un 5% al flujo de la cuenca del Tinguiririca en Bajo los Briones, y en 2019 representó el 39% del flujo estival. Esta contribución es significativa, considerando que el río Tinguiririca proporciona agua potable a 100,000 personas y respalda actividades económicas vitales como la generación de energía hidroeléctrica y valles altamente productivos como el Valle de Colchagua, conocido por su producción de vino.

Como dirección futura de investigación, se sugiere investigar más a fondo los efectos de la calibración con balances de masa geodésicos utilizando diferentes fuentes de datos para los mismos periodos temporales. Este enfoque ayudará a abordar las consecuencias de las fortalezas y debilidades de cada método empleado y mejorará la precisión y confiabilidad de los resultados de las simulaciones.

BIBLIOGRAFÍA

Ahmed R, Wani GF, Ahmad ST, Sahana M, Singh H and Ahmed P (2021) A review of glacial lake expansion and associated glacial lake outburst floods in the himalayan region (doi: 10.1007/s41748-021-00230-9).

Anderson ER (2017) Modelling changes in multi-decadal streamflow contributions – bologna glacier, selwyn mountains, nwt, canada

Annandale J, Jovanovic N, Benad N and Allen R (2002) Software for missing data error analysis of penman-monteith reference evapotranspiration. Irrigation Science, 21, 57–67, ISSN 0342-7188 (doi: 10.1007/s002710100047)

Ayala A, Pellicciotti F, MacDonell S, McPhee J, Vivero S, Campos C and Egli P (2016) Modelling the hydrological response of debris-free and debris-covered glaciers to present climatic conditions in the semiarid andes of central chile. Hydrological Processes, 30, 4036–4058, ISSN 10991085 (doi: 10.1002/hyp.10971)

Ayala Farías-Barahona D, Huss M, Pellicciotti F, McPhee J and Farinotti D (2020) Glacier runoff variations since
1955 in the maipo river basin, in the semiarid andes of central chile. Cryosphere, 14, 2005–2027, ISSN 19940424 (doi: 10.5194/tc-14-2005-2020)

Barandun M, Bravo C, Grobety B, Jenk T, Fang L, Naegeli K, Rivera A, Cisternas S, Münster T and Schwikowski M (2022) Anthropogenic influence on surface changes at the olivares glaciers; central chile. Science of the Total Environment, 833, ISSN 18791026 (doi: 10.1016/j.scitotenv.2022.155068)

Barcaza G, Nussbaumer SU, Tapia G, Valdés J, García JL, Videla Y, Albornoz A and Arias V (2017) Glacier inventory and recent glacier variations in the andes of chile, south america. Annals of Glaciology, 58, 166–180, ISSN 02603055 (doi: 10.1017/aog.2017.28)

Barria I, Carrasco J, Casassa G and Barria P (2019) Simulation of long-term changes of the equilibrium line altitude in the central chilean andes mountains derived from atmospheric variables during the 1958–2018 period. Frontiers in Environmental Science, 7, ISSN 2296665X (doi: 10.3389/fenvs.2019.00161)

Behrangi A, Yin X, Rajagopal S, Stampoulis D and Ye H (2018) On distinguishing snowfall from rainfall using near-surface atmospheric information: Comparative analysis, uncertainties and hydrologic importance. Quarterly Journal of the Royal Meteorological Society, 144, 89–102, ISSN 1477870X (doi: 10.1002/qj.3240)

Bernhardt M and Schulz K (2010) Snowslide: A simple routine for calculating gravitational snow transport. Geophysical Research Letters, 37, ISSN 00948276 (doi: 10.1029/2010GL043086)

Boisier JP, Rondanelli R, Garreaud RD and Muñoz F (2016) Anthropogenic and natural contributions to the southeast pacific precipitation decline and recent megadrought in central chile. Geophysical Research Letters, 43, 413–421, ISSN 19448007 (doi: 10.1002/2015GL067265)

Braithwaite RJ and Hughes PD (2020) Regional geography of glacier mass balance variability over seven decades 1946–2015. Frontiers in Earth Science, 8, ISSN 22966463 (doi: 10.3389/feart.2020.00302)

Braun MH, Malz P, Sommer C, Farías-Barahona D, Sauter T, Casassa G, Soruco A, Skvarca P and Seehaus TC (2019) Constraining glacier elevation and mass changes in south america. Nature Climate Change, 9, 130–136, ISSN 17586798 (doi: 10.1038/s41558-018-0375-7)

Bravo C, Loriaux T, Rivera A and Brock BW (2017) Assessing glacier melt contribution to streamflow at universidad glacier, central andes of chile. Hydrology and Earth System Sciences, 21, 3249–3266, ISSN 16077938 (doi:10.5194/hess-21-3249-2017)

Burger F, Brock B and Montecinos A (2018) Seasonal and elevational contrasts in temperature trends in central chile between 1979 and 2015. Global and Planetary Change, 162, 136–147, ISSN 09218181 (doi: 10.1016/j.gloplacha.2018.01.005)

Burger F, Ayala A, Farias D, Shaw TE, MacDonell S, Brock B, McPhee J and Pellicciotti F (2019) Interannual variability in glacier contribution to runoff from a high-elevation andean catchment: understanding the role of debris cover in glacier hydrology. Hydrological Processes, 33, 214–229, ISSN 10991085 (doi: 10.1002/hyp.13354)

Cannon AJ (2018) Multivariate quantile mapping bias correction: an n-dimensional probability density function transform for climate model simulations of multiple variables. Climate Dynamics, 50, 31–49, ISSN 14320894 (doi: 10.1007/s00382-017-3580-6)

Carenzo M, Pellicciotti F, Mabillard J, Reid T and Brock BW (2016) An enhanced temperature index model for debris-covered glaciers accounting for thickness effect. Advances in Water Resources, 94, 457–469, ISSN 03091708 (doi: 10.1016/j.advwatres.2016.05.001)

Caretta MA, Mukherji A, Arfanuzzaman M, Betts RA, Gelfan A, Hirabayashi Y, Lissner TK, Liu J, Gunn EL, Morgan R, Mwanga S, Supratid S, Pörtner HO, Roberts DC, Tignor M, Poloczanska ES, Mintenbeck K, Alegría A, Craig M, Langsdorf S, Löschke S, Möller V, Okem A and Rama B (2020) 2022: Water. in: Climate change 2022: Impacts, adaptation and vulnerability. contribution of working group ii to the sixth assessment report of the intergovernmental panel on climate change. Cambridge University Press (doi: 10.1017/9781009325844.006)

Compagno L, Huss M, Miles ES, McCarthy MJ, Zekollari H, Dehecq A, Pellicciotti F and

Farinotti D (2022) Modelling supraglacial debris-cover evolution from the single-glacier to the regional scale: an application to high mountain asia. Cryosphere, 16, 1697–1718, ISSN 19940424 (doi: 10.5194/tc-16-1697-2022)

Cuffey KM and Paterson WSB (2010) The Physics of Glaciers Fourth Edition. ISBN 9780123694614

Dai A (2008) Temperature and pressure dependence of the rain-snow phase transition over land and ocean. Geophysical Research Letters, 35, ISSN 00948276 (doi: 10.1029/2008GL033295)

DGA, Casassa G, Espinoza A, Segovia A and Huenante J (2022) MetodologÍa del inventario pÚblico de glaciares, sdt n°447, 2022

Duan Q, Sorooshian S and Gupta V (1992) Effective and efficient global optimization for conceptual rainfall-runoff models

Dussaillant I, Berthier E, Brun F, Masiokas M, Hugonnet R, Favier V, Rabatel A, Pitte P and Ruiz L (2019) Two decades of glacier mass loss along the andes. Nature Geoscience, 12, 802–808, ISSN 17520908 (doi: 10.1038/s41561019-0432-5)

Escanilla-Minchel R, Alcayaga H, Soto-Alvarez M, Kinnard C and Urrutia R (2020) Evaluation of the impact of climate change on runoff generation in an andean glacier watershed. Water, 12, 3547, ISSN 2073-4441 (doi: 10.3390/w12123547)

Essery R (2004) Parameter sensitivity in simulations of snowmelt. Journal of Geophysical Research, 109, D20111, ISSN 0148-0227 (doi: 10.1029/2004JD005036)

Farías-Barahona D, Vivero S, Casassa G, Schaefer M, Burger F, Seehaus T, Iribarren-Anacona P, Escobar F and Braun MH (2019) Geodetic mass balances and area changes of echaurren norte glacier (central andes, chile) between 1955 and 2015. Remote Sensing, 11, ISSN 20724292 (doi: 10.3390/rs11030260)

Fealy R and Sweeney J (2005) Detection of a possible change point in atmospheric variability in the north atlantic and its effect on scandinavian glacier mass balance. International Journal of Climatology, 25, 1819–1833, ISSN 08998418 (doi: 10.1002/joc.1231)

Frans C, Istanbulluoglu E, Lettenmaier DP, Fountain AG and Riedel J (2018) Glacier recession and the response of summer streamflow in the pacific northwest united states, 1960–2099. Water Resources Research, 54, 6202–6225, ISSN 19447973 (doi: 10.1029/2017WR021764)

Fugazza D, Senese A, Azzoni RS, Maugeri M and Diolaiuti GA (2016) Spatial distribution of surface albedo at the forni glacier (stelvio national park, central italian alps). Cold Regions Science and Technology, 125, 128–137, ISSN 0165232X (doi: 10.1016/j.coldregions.2016.02.006)

Gabbi J, Carenzo M, Pellicciotti F, Bauder A and Funk M (2014) A comparison of empirical and physically based glacier surface melt models for long-term simulations of glacier response. Journal of Glaciology, 60, 1199–1207, ISSN 00221430 (doi: 10.3189/2014JoG14J011)

Garnier BJ and Ohmura A (1970) The evaluation of surface variations in solar radiation income. Solar Energy, 13, 21–34, ISSN 0038092X (doi: 10.1016/0038-092X(70)90004-6)

Garreaud RD, Alvarez-Garreton C, Barichivich J, Boisier JP, Christie D, Galleguillos M, LeQuesne C, McPhee J and Zambrano-Bigiarini M (2017) The 2010-2015 megadrought in central chile: Impacts on regional hydroclimate and vegetation. Hydrology and Earth System Sciences, 21, 6307–6327, ISSN 16077938 (doi: 10.5194/hess-21-6307-2017)

Garreaud RD, Boisier JP, Rondanelli R, Montecinos A, Sepúlveda HH and Veloso-Aguila D (2020) The central chile mega drought (2010–2018): A climate dynamics perspective. International Journal of Climatology, 40, 421–439, ISSN 10970088 (doi: 10.1002/joc.6219)

Granger RJ and Gray DM (1989) Evaporation from natural nonsaturated surfaces

Gray DM and Granger RJ (1986) In situ measurements of moisture and salt movement in freezing soils

Hall DK, Riggs GA, Salomonson VV, DiGirolamo NE and Bayr KJ (2002) Modis snow-cover products. Remote Sensing of Environment, 83, 181–194, ISSN 00344257 (doi: 10.1016/S0034-4257(02)00095-0)

Herron MM and Langway CC (1980) Firn densification: An empirical model. Journal of Glaciology, 25, 373–385, ISSN 0022-1430 (doi: 10.3189/s0022143000015239)

Hugonnet R, McNabb R, Berthier E, Menounos B, Nuth C, Girod L, Farinotti D, Huss M, Dussaillant I, Brun F and

Kääb A (2021) Accelerated global glacier mass loss in the early twenty-first century. Nature, 592, 726–731, ISSN 14764687 (doi: 10.1038/s41586-021-03436-z)

Huss M and Hock R (2018) Global-scale hydrological response to future glacier mass loss. Nature Climate Change, 8, 135–140, ISSN 17586798 (doi: 10.1038/s41558-017-0049-x)

Huss M, Jouvet G, Farinotti D and Bauder A (2010) Future high-mountain hydrology: A new parameterization of glacier retreat. Hydrology and Earth System Sciences, 14, 815–829, ISSN 10275606 (doi: 10.5194/hess-14-815-2010)

Immerzeel WW, Lutz AF, Andrade M, Bahl A, Biemans H, Bolch T, Hyde S, Brumby S,

Davies BJ, Elmore AC, Emmer A, Feng M, Fernández A, Haritashya U, Kargel JS, Koppes M, Kraaijenbrink PD, Kulkarni AV, Mayewski

PA, Nepal S, Pacheco P, Painter TH, Pellicciotti F, Rajaram H, Rupper S, Sinisalo A, Shrestha AB, Viviroli D, Wada Y, Xiao C, Yao T and Baillie JE (2020) Importance and vulnerability of the world's water towers. Nature, 577, 364–369, ISSN 14764687 (doi: 10.1038/s41586-019-1822-y)

Jara F, Lagos-Zúñiga M, Fuster R, Mattar C and McPhee J (2021) Snow processes and climate sensitivity in an arid mountain region, northern chile. Atmosphere, 12, ISSN 20734433 (doi: 10.3390/atmos12040520)

Kinnard C, MacDonell S, Petlicki M, Martinez CM, Aberman J and Urrutia R (2018) Mass balance and meteorological conditions at universidad glacier, central chile

Kinnard C, Ginot P, Surazakov A, MacDonell S, Nicholson L, Patris N, Rabatel A, Rivera A and Squeo FA (2020) Mass balance and climate history of a high-altitude glacier, desert andes of chile. Frontiers in Earth Science, 8, ISSN 22966463 (doi: 10.3389/feart.2020.00040)

Li F, Maussion F, Wu G, Chen W, Yu Z, Li Y and Liu G (2023) Influence of glacier inventories on ice thickness estimates and future glacier change projections in the tian shan range, central asia. Journal of Glaciology, 69, 266–280, ISSN 0022-1430 (doi: 10.1017/jog.2022.60)

Lliboutry L (1958) Studies of the shrinkage after a sudden advance, blue bands and wave ogives on glaciar universidad (central chilean andes). Journal of Glaciology, 3, 261–270, ISSN 0022-1430 (doi: 10.3189/s002214300002390x) Macdonell S, Kinnard C, Mölg T, Nicholson L and Abermann J (2013) Meteorological drivers of ablation processes on a cold glacier in the semi-arid andes of chile. Cryosphere, 7, 1513–1526, ISSN 19940416 (doi: 10.5194/tc-71513-2013)

Malmros JK, Mernild SH, Wilson R, Tagesson T and Fensholt R (2018) Snow cover and snow albedo changes in the central andes of chile and argentina from daily modis observations (2000–2016). Remote Sensing of Environment, 209, 240–252, ISSN 00344257 (doi: 10.1016/j.rse.2018.02.072)

Marcoleta L (2019) Hidro-glaciologÍa de glaciares rocosos y descubiertos en los

Marks D, Kimball J, Tingey D and Link T (1998) The sensitivity of snowmelt processes to climate conditions and forest cover during rain-on-snow: a case study of the 1996 pacific northwest

Marzeion B, Kaser G, Maussion F and Champollion N (2018) Limited influence of climate change mitigation on short-term glacier mass loss. Nature Climate Change, 8, 305–308, ISSN 17586798 (doi: 10.1038/s41558-018-0093-1)

Masiokas MH, Christie DA, Quesne CL, Pitte P, Ruiz L, Villalba R, Luckman BH, Berthier E, Nussbaumer SU, Álvaro González-Reyes, McPhee J and Barcaza G (2016) Reconstructing the annual mass balance of the echaurren norte glacier (central andes, 33.5° s) using local and regional hydroclimatic data. Cryosphere, 10, 927–940, ISSN 19940424 (doi: 10.5194/tc-10-927-2016)

Masiokas MH, Rabatel A, Rivera A, Ruiz L, Pitte P, Ceballos JL, Barcaza G, Soruco A, Bown F, Berthier E, Dussaillant I and MacDonell S (2020) A review of the current state and recent changes of the andean cryosphere. Frontiers in Earth Science, 8, ISSN 22966463 (doi: 10.3389/feart.2020.00099)

Medwedeff WG and Roe GH (2017) Trends and variability in the global dataset of glacier mass balance. Climate Dynamics, 48, 3085–3097, ISSN 14320894 (doi: 10.1007/s00382-016-3253-x)

Oerlemans J and Klok EJ (2004) Effect of summer snowfall on glacier mass balance. Annals of Glaciology, 38, 97–100, ISSN 02603055 (doi: 10.3189/172756404781815158)

Orrego F, American A, Ascanio R and Ginocchio R (2021) ECOSISTEMAS DE MONTAÑA DE LA CUENCA ALTA DEL RÍO MAPOCHO. ISBN 978-956-404-94 8

Pellicciotti F, Ragettli S, Carenzo M and McPhee J (2014) Changes of glaciers in the andes of chile and priorities for future work (doi: 10.1016/j.scitotenv.2013.10.055)

Peña H and Nazarala B (1987) Snowmelt - runoff simulation model of a central chile andean basin with relevant orographic effects. 161–173

Pomeroy J, Brown T, Fang X, Shook K, Pradhananga D, Armstrong R, Harder P, Marsh C, Costa D, Krogh S, Aubry-Wake C, Annand H, Lawford P, He Z, Kompanizare M and Moreno JL (2022) The cold regions hydrological modelling platform for hydrological diagnosis and prediction based on process understanding. Journal of Hydrology, 615, 128711, ISSN 00221694 (doi: 10.1016/j.jhydrol.2022.128711)

Pomeroy JW (1997) Sustainability of the western canadian boreal forest under changing hydrological conditions-2summer energy and water use snowmip (snow model intercomparison project)-snowmip, snowmip2, esm-snowmip view project changing cold regions network (ccrn) view project

Pomeroy JW and Li L (2000) Prairie and arctic areal snow cover mass balance using a blowing snow model. Journal of Geophysical Research Atmospheres, 105, 26619–26634, ISSN 01480227 (doi: 10.1029/2000JD900149)

Pomeroy JW, Gray DM and Landine PG (1993) The prairie blowing snow model: characteristics, validation, operation

Pomeroy JW, Gray DM, Brown T, Hedstrom NR, Quinton WL, Granger RJ and Carey SK

(2007) The cold regions hydrological model: a platform for basing process representation and model structure on physical evidence. Hydrological Processes, 21, 2650–2667, ISSN 08856087 (doi: 10.1002/hyp.6787)

Pradhananga D (2020) Response of canadian rockies glacier hydrologyto changing climate

Pradhananga D and Pomeroy JW (2022) Diagnosing changes in glacier hydrology from physical principles using a hydrological model with snow redistribution, sublimation, firnification and energy balance ablation algorithms. Journal of Hydrology, 608, ISSN 00221694 (doi: 10.1016/j.jhydrol.2022.127545)

Ragettli S, Cortés G, Mcphee J and Pellicciotti F (2014) An evaluation of approaches for modelling hydrological processes in high-elevation, glacierized andean watersheds. Hydrological Processes, 28, 5674–5695, ISSN 10991085 (doi: 10.1002/hyp.10055)

Ragettli S, Immerzeel WW and Pellicciotti F (2016) Contrasting climate change impact on river flows from highaltitude catchments in the himalayan and andes mountains. Proceedings of the National Academy of Sciences of the United States of America, 113, 9222–9227, ISSN 10916490 (doi: 10.1073/pnas.1606526113)

Rakovec O, Hill MC, Clark MP, Weerts AH, Teuling AJ and Uijlenhoet R (2014) Distributed evaluation of local sensitivity analysis (delsa), with application to hydrologic models. Water Resources Research, 50, 409–426, ISSN 00431397 (doi: 10.1002/2013WR014063)

Shaw TE, Ulloa G, Farías-Barahona D, Fernandez R, Lattus JM and McPhee J (2021) Glacier albedo reduction and drought effects in the extratropical andes, 1986-2020. Journal of Glaciology, 67, 158–169, ISSN 00221430 (doi: 10.1017/jog.2020.102)

Sicart JE, Pomeroy JW, Essery RL and Bewley D (2006) Incoming longwave radiation to melting snow: Observations, sensitivity and estimation in northern environments. Hydrological Processes, 20, 3697–3708, ISSN 08856087 (doi: 10.1002/hyp.6383)

Ultee L, Coats S and Mackay J (2022) Glacial runoff buffers droughts through the 21st century. Earth System Dynamics, 13, 935–959, ISSN 21904987 (doi: 10.5194/esd-13-935-2022)

Verseghy DL (1991) Class-a canadian land surface scheme for gcms. i. soil model

Wilson R, Mernild SH, Malmros JK, Bravo C and Carrión D (2016) Surface velocity fluctuations for glaciar universidad, central chile, between 1967 and 2015. Journal of Glaciology, 62, 847–860, ISSN 00221430 (doi: 10.1017/jog.2016.73)

Zekollari H, Huss M, Farinotti D and Lhermitte S (2022) Ice-dynamical glacier evolution modeling—a review (doi: 10.1029/2021RG000754)

Zemp M, Frey H, Gärtner-Roer I, Nussbaumer SU, Hoelzle M, Paul F, Haeberli W,

Denzinger F, Ahlstrøm AP, Anderson B, Bajracharya S, Baroni C, Braun LN, Càceres BE, Casassa G, Cobos G, Dàvila LR, Granados HD,

Demuth MN, Espizua L, Fischer A, Fujita K, Gadek B, Ghazanfar A, Hagen JO, Holmlund P, Karimi N, Li Z, Pelto M, Pitte P, Popovnin VV, Portocarrero CA, Prinz R, Sangewar CV, Severskiy I, Sigurdsson O, Soruco A, Usubaliev R and Vincent C (2015) Historically unprecedented global glacier decline in the early 21st century. Journal of Glaciology, 61, 745–762, ISSN 00221430 (doi: 10.3189/2015JoG15J017)

Zemp M, Huss M, Thibert E, Eckert N, McNabb R, Huber J, Barandun M, Machguth H, Nussbaumer SU, GärtnerRoer I, Thomson L, Paul F, Maussion F, Kutuzov S and Cogley JG (2019) Global glacier mass changes and their contributions to sea-level rise from 1961 to 2016. Nature, 568, 382–386, ISSN 14764687 (doi: 10.1038/s41586-0191071-0)